INERTIALLY DERIVED FLYING QUALITIES AND PERFORMANCE PARAMETERS

NAVAL TEST PILOT SCHOOL

16 JUNE 1976

TM-TPS 76-1

Technical Memorandum

INERTIALLY DERIVED FLYING QUALITIES AND PERFORMANCE PARAMETERS

LCDR W. C. Bowes
Mr. R. V. Miller

16 June 1976

NAVAL AIR TEST CENTER
PATUXENT RIVER, MARYLAND

UNCLASSIFIED

SECURITY CLASSIFICATION OF THIS PAGE (When Data Entered)

REPORT DOCUMENTATION PAGE		READ INSTRUCTIONS BEFORE COMPLETING FORM
1 REPORT NUMBER TM-TPS 76-1	2 GOVT ACCESSION NO	3 RECIPIENT'S CATALOG NUMBER
4 TITLE (and Subtitle) INERTIALLY DERIVED FLYING QUALITIES AND PERFORMANCE PARAMETERS		5 TYPE OF REPORT & PERIOD COVERED 6 PERFORMING ORG REPORT NUMBER
7 AUTHOR(s) LCDR W. C. BOWES MR. R. V. MILLER		8 CONTRACT OR GRANT NUMBER(s)
9 PERFORMING ORGANIZATION NAME AND ADDRESS NAVAL AIR TEST CENTER NAVAL AIR STATION PATUXENT RIVER, MARYLAND 20670		10 PROGRAM ELEMENT PROJECT TASK AREA & WORK UNIT NUMBERS
11 CONTROLLING OFFICE NAME AND ADDRESS		12 REPORT DATE 16 JUNE 1976 13 NUMBER OF PAGES 77
14 MONITORING AGENCY NAME & ADDRESS(if different from Controlling Office)		15 SECURITY CLASS (of this report) UNCLASSIFIED 15a DECLASSIFICATION DOWNGRADING SCHEDULE

16 DISTRIBUTION STATEMENT (of this Report)

APPROVED FOR PUBLIC RELEASE; DISTRIBUTION UNLIMITED

17 DISTRIBUTION STATEMENT (of the abstract entered in Block 20, if different from Report)

18 SUPPLEMENTARY NOTES

19 KEY WORDS (Continue on reverse side if necessary and identify by block number)

FLIGHT TESTING	STABILITY AND CONTROL TESTING
INSTRUMENTATION	DYNAMIC PERFORMANCE TESTING
INERTIAL NAVIGATION SYSTEMS	FLIGHT TEST TECHNIQUES
FLYING QUALITIES TESTING	AIRCRAFT STABILITY
PERFORMANCE TESTING	AIRCRAFT PERFORMANCE

20 ABSTRACT (Continue on reverse side if necessary and identify by block number)

A feasibility study was undertaken at the U. S. Naval Test Pilot School (USNTPS) in which an inertial navigation system in an A-7C airplane was successfully utilized to derive the conventional flying qualities and performance parameters which are used to describe an aircraft's motion.

This report presents a discussion on the theoretical and practical aspects of utilizing an inertial navigation system in flying qualities and performance testing. Also presented are some of the data obtained during the feasibility study and a discussion of the numerous

DD FORM 1 JAN 73 1473 EDITION OF 1 NOV 65 IS OBSOLETE

UNCLASSIFIED

PRICES SUBJECT TO CHANGE

20.

advantages of utilizing this concept for flight testing. The data obtained were extremely accurate, and the cost of instrumenting USNTPS A-7C airplanes was reduced significantly (in terms of dollars and aircraft down time) from utilizing the conventional flight test instrumentation method.

PREFACE

A feasibility study was undertaken at the U. S. Naval Test Pilot School (USNTPS) to develop a method of instrumenting the USNTPS A-7C airplanes for flying qualities and performance testing while retaining the airplanes' full weapon systems capability. An additional purpose of this study was to minimize the cost and the length of time required to instrument an airplane for conventional flying qualities and performance testing. This technical memorandum presents the results of this feasibility study. The work was conducted as an integral part of the mission of USNTPS under NAVAIRSYSCOM AIRTASK A510-610C/053-F/6WSL71-0000 of 2 December 1975.

APPROVED FOR RELEASE

R. A. JOHNSON, CDR, USN
DIRECTOR
U. S. NAVAL TEST PILOT SCHOOL

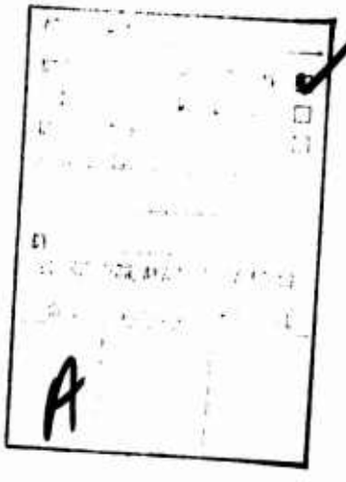

TABLE OF CONTENTS

LIST OF ILLUSTRATIONS

LIST OF TABLES

INTRODUCTION

BACKGROUND

1. A program was undertaken at the U. S. Naval Test Pilot School (USNTPS) to determine the feasibility of using inertially derived data to generate the attitude, attitude rate, acceleration, and velocity data required to describe aircraft motion for traditional flying qualities and performance testing. The main impetus for pursuing this program at USNTPS was in trying to retain a full weapons system capability in an A-7C airplane while also being able to utilize the airplane for Test Pilot School flying qualities and performance testing. Trying to incorporate the currently utilized rate gyros, attitude sensors, accelerometers, and the associated signal conditioning, etc., would have compromised the A-7C's full system capability, and the cost, in terms of dollars and aircraft down time, would have been high.

2. For many years aircraft have been operating with highly accurate and reliable inertial navigation systems. When one looks at the required accuracies of the measured accelerations and attitudes from an inertial system that navigates with a circular error probable (CEP) rate of 1 to 2 nmi/hr (1.9 to 3.7 km/hr), one finds acceleration accuracies of mili g's and attitude accuracies of arc minutes. These accuracies are orders of magnitude better than accuracies with conventional instrumentation.

3. This program was not the first attempt to utilize an inertial system for aircraft flight testing. The General Dynamics YF-16 Flight Test Program utilized a modified Delco Carousel V inertial platform for performance testing (reference 1), but General Dynamics did not utilize the inertial platform for stability and control testing. This platform is not one that will be incorporated in the production F-16 airplane. General Dynamics was highly successful in this venture and will again utilize this inertial system for the performance testing of the preproduction F-16 airplanes. Reference 1 discusses the use of an inertial system for the performance testing of the YF-16 and should be required reading for anyone intending to use an inertial system for flight testing.

PURPOSE

4. The purpose of this feasibility study was to determine if an inertial navigation system could be utilized to derive the conventional flying qualities and performance parameters which are used to describe an aircraft's motion.

DESCRIPTION OF TEST AIRCRAFT

5. A production A-7C airplane was used for the feasibility study, and it was an excellent vehicle with which to pursue an inertially derived flying qualities and performance parameters (IFP) program. Even more important was the availability of an A-7C airplane that had been utilized during the A-7C/E weapons system development. This airplane had the capability of recording or telemetering 99 parameters from its on-board computer. Included in these parameters were those parameters required to verify the feasibility and accuracy of an IFP system.

6. The A-7C airplane incorporates a relatively sophisticated navigation and weapons delivery system. An ASN-91 Tactical Computer (a Four Pi IBM solid state general purpose digital computer) and an ASN-90 Inertial Measurement Unit and Adaptive Power Supply (built by Singer Kearfott) are the major components of the airplane's inertial system.

7. One of the circuit boards (pages is the IBM term) in the airplane's tactical computer was modified to enable the recording of the parameters of interest. An intermediate bandwidth tape recorder to record a 50 kilo bit signal was also installed in the airplane. Since this initial program was undertaken only to prove the concept of IFP, no additional instrumentation was installed in the airplane. Therefore, cockpit control forces, control surface positions, and engine performance parameters were not available during this initial feasibility program.

8. The A-7C tactical computer has a sample rate of 25 times per sec for most parameters (all inertial parameters) and five times per sec for others. Table I lists the recorded parameters that were utilized for this evaluation and their corresponding sample rates. Of the 99 parameters from the tactical computer that are recorded on one track of the tape recorder, only 18 were utilized in this program.

Table I

Parameters Recorded in Flight

Parameter	Sample Rate (Times/Sec)	Units	Remarks
Time	25	sec	
Identification	5	-	A one (1) appears on printout when target designate feature is activated; serves same purpose as "p" light.
Event Number	5	-	The pilot selects the desired event number by selecting the number of bombs (0 to 99) on Armament Release Panel.
Inertial Velocity North (V_{NI})	25	fps	
Inertial Velocity East (V_{EI})	25	fps	
Inertial Velocity Vertical (V_{VI})	25	fps	
Sine of Platform Pitch Angle (Sin θ)	25	-	This was the only form in which pitch was available from the computer.
Sine of Platform Roll Angle (Sin ϕ)	25	-	This was the only form in which roll was available from the computer.
Platform Yaw Angle (ψ)	5	deg	
Vane Angle of Attack (α)	5	deg	From production angle of attack vane.
Pressure Altitude (Hp)	5	ft	Air data computer (ADC) output.
True Airspeed (V_A)	5	fps	ADC output.
Smooth Winds East (V_{WE})	5	fps	Computed by tactical computer.
Smooth Winds North (V_{WN})	5	fps	Computed by tactical computer.
Magnetic Heading	5	deg	
Mach Number	5	-	
Air Density	5	$slug/ft^3$	
Weight on Gear	5	-	

9. The ASN-90 is a four gimbaled North pointing inertial measurement unit which incorporates integrating accelerometers. Previous test data have shown the system to navigate with a mean circular error probable of 1.75 nmi/hr (3 241 m/hr) when operated in the pure inertial mode (reference 2). The inertial system incorporates a doppler damping feature that was not utilized because of its poorer performance than the pure inertial mode.

10. A long-term vertical velocity damping feature utilizing the air data computer unit is incorporated, but it has essentially no effect on short-term inertial vertical velocity errors. It does, however, keep the d. c. or long-term value of vertical velocity from increasing with time.

11. The IMU is rigidly mounted and accurately boresighted to the body axis of the airplane. The outer roll gimbal of the IMU is shock mounted to the IMU case in order to attenuate high frequency vibrations and to provide some mechanical protection to the unit. The IMU accurately measures accelerations up to a nominal input frequency of 20 cycles per sec.

12. Since integrating accelerometers are utilized in the IMU, a velocity vice an acceleration output is obtained. The integrating accelerometers serve a secondary function of attenuating high frequency vibrations.

SCOPE OF THE TESTS

13. Two flights for a total of 3.3 flight hours were flown. On the first flight the inertial navigation system (INS) had a failure and navigated with a 23 nmi/hr (43 000 m/hr) error. The flight was therefore repeated after the INS had been repaired. On the second flight, the navigation error was 3 miles (5 500 m) after 1.8 hours.

RESULTS OF THE STUDY

ATTAINABLE PARAMETERS

14. An inertial system presents attitudes and accelerations (velocities if integrating accelerometers are utilized) in relation to its three orthogonal axes which are maintained stable to a desired coordinate system. Typically, this is an earth-referenced "local vertical" system having one axis of the coordinate system pointed North, one East, and one vertical.

15. In flight test work, an earth-referenced coordinate system is utilized when discussing an aircraft's attitude. However, an orthogonal reference system coinciding with the aircraft's body axis is utilized when working with attitude rates, accelerations, velocities, angle of attack, and sideslip. Figure 1 shows the earth-referenced coordinate system and the aircraft body-axis coordinate system.

EARTH-REFERENCED
COORDINATE SYSTEM
V
N
W
AIRCRAFT BODY-AXIS
COORDINATE SYSTEM
TPS
Y
LATERAL AXIS
q - PITCH RATE
X
LONGITUDINAL
AXIS
P
ROOL RATE
r - YAW RATE
Z
VERTICAL AXIS

16. In flight test work, aircraft motion (a vector) is described in terms of three components in the orthogonal triad coinciding with the aircraft's body axes. Since the inertial system presents aircraft motion in relation to an earth-referenced orthogonal triad, it is necessary to transform the three coordinates of the aircraft motion vector from the earth-referenced frame to the aircraft's axis referenced frame.

17. To further illustrate the need for this transformation, take the example of an airplane executing a turn with 90 deg of right bank angle and its nose fixed on the horizon. The inertial system would show a platform reference pitch rate ($\dot{\theta}$) of zero and a positive platform reference right yaw rate ($\dot{\psi}$). However, flight test convention would describe this airplane as having a positive body axis pitch rate (q) and a body axis yaw rate (r) of zero.

18. Euler angles were utilized to transform vectors from the earth-referenced axis system to the aircraft's body axis system. Any possible rotational sequence could have been utilized, but since aircraft inertial systems have their gimbals arranged from inside to out as yaw, pitch, and roll, the first rotation for the transformation was about the platform vertical axis (i.e., rotating in azimuth). The next rotation was in platform pitch and the last in platform roll. It is important to always utilize the same order of rotation to describe the attitude of the aircraft. With a conventional aircraft INS, this will always be yaw, pitch, then roll.

19. Since flight test work references aircraft motion to the air mass, earth-referenced velocities must be converted to air mass reference velocities. The respective North and East component of the wind is added to North and East inertial velocities prior to the transformation to body axis velocities. It is assumed that the wind lay only in the horizontal plane and that the vertical component of wind is equal to zero.

AIR MASS REFERENCED VELOCITIES AND ANGLES

20. Figure 2 presents in block diagram format the calculations that were made to the INS and air data computer (ADC) outputs in order to obtain the air mass referenced velocities along the aircraft's three orthogonal body axes. The following definitions were used:

V_{NI}, V_{EI}, V_{VI}	are the true North, East, and vertical inertial velocities obtained from the INS.
V_{WN}, V_{WE}	are the true North and East wind velocities as calculated by the tactical computer by comparing inertial velocities with the true airspeed from the ADC.
θ, ϕ, ψ	are the earth-referenced pitch, roll, and yaw angles of the aircraft as measured by the INS (i.e., platform pitch, roll, and yaw angles).

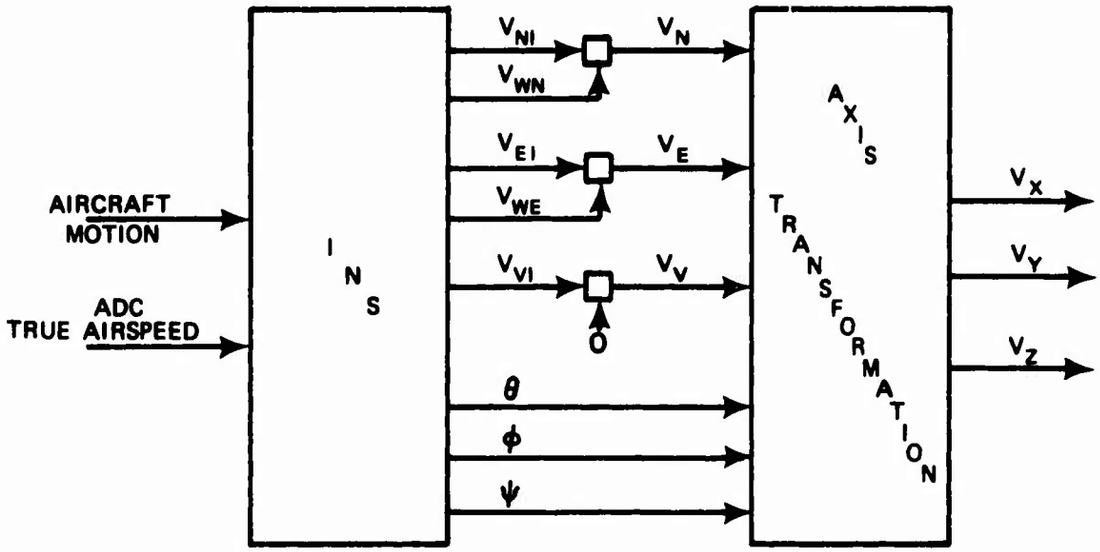

Figure 2
Transformation Block Diagrams

21. The INS inertial velocities (V_{NI}, V_{EI}) were combined with the tactical computer's calculated winds (V_{WN}, V_{WE}) to give the air mass referenced velocities V_N, V_E, and V_V. It was assumed that the vertical wind component was zero. Therefore, the air mass referenced vertical velocity (V_V) was assumed equal to the inertial vertical velocity (V_{VI}).

22. With the air mass referenced velocities computed and the earth-referenced platform attitudes available from the INS, the next step was to determine the air mass velocities relative to the aircraft's body axis coordinate system. The matrix (reference 3) used for this transformation is given below:

$$\begin{vmatrix} V_x \\ V_y \\ V_z \end{vmatrix} = \begin{vmatrix} \cos\psi\cos\theta & \sin\psi\cos\theta & -\sin\theta \\ \cos\psi\sin\theta\sin\phi - \sin\psi\cos\phi & \sin\psi\sin\theta\sin\phi + \cos\psi\cos\phi & \cos\theta\sin\phi \\ \cos\psi\sin\theta\cos\phi + \sin\psi\sin\phi & \sin\psi\sin\theta\cos\phi - \cos\psi\sin\phi & \cos\theta\cos\phi \end{vmatrix} \begin{vmatrix} V_N \\ V_E \\ V_V \end{vmatrix}$$

The solution for V_x, V_y, and V_z is then as follows:

$$V_x = V_N \cos\psi\cos\theta + V_E \sin\psi\cos\theta - V_V \sin\theta$$

$$V_y = V_N (\cos\psi\sin\theta\sin\phi - \sin\psi\cos\phi) + V_E (\sin\psi\sin\theta\sin\phi + \cos\psi\cos\phi) + V_V \cos\theta\sin\phi$$

$$V_z = V_N (\cos\psi\sin\theta\cos\phi + \sin\psi\sin\phi) + V_E (\sin\psi\sin\theta\cos\phi - \cos\psi\sin\phi) + V_V \cos\theta\cos\phi$$

23. The next series of computations, illustrated by figure 3, determined the orientation of the relative wind with respect to the aircraft body axis coordinate system. These computations were utilized to determine angle of attack, α, sideslip angle, β, and flight path angle, γ.

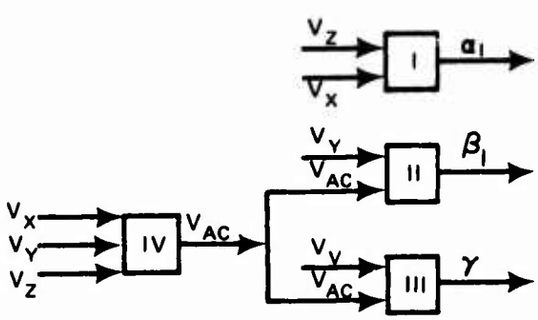

I. $\alpha_I = \tan^{-1}\left(V_Z/V_X\right)$

II. $\beta_I = \sin^{-1}\left[\frac{V_Y}{V_{AC}}\right]$

III. $\gamma = \sin^{-1}\left(\frac{V_v}{V_{AC}}\right)$

IV. $V_{AC} = \sqrt{V_x^2 + V_y^2 + V_z^2}$

Figure 3
α, β, γ Determination Block Diagrams

24. During dynamic maneuvers, rapid accelerations/decelerations, transonics, sideslips, and normal accelerations other than one, static source position error and pitot static system lags can cause appreciable errors in the true airspeed derived by the ADC. It is for this reason that the computed winds were "frozen" in the beginning of most data gathering maneuvers, and a "corrected true airspeed" (V_{AC}) was calculated for the computation of β and γ. The mean of the wind readouts during the previous 5 sec prior to freezing the wind was utilized as the magnitude and direction of the frozen wind. Since the frozen value of the wind was used for the calculation of V_x and V_y, the computed angle of attack was not subjected to the pitot static measurement errors which occur during the various maneuvers.

25. The calculation of winds by the A-7's on-board computer assumes that the aircraft is in zero sideslip (i.e., the true airspeed vector is assumed as being attached to the aircraft's nose). It was therefore necessary to trim the airplane for zero sideslip at the beginning of each maneuver prior to freezing the winds. In a symmetrically loaded airplane with good side force characteristics ($dC_Y/d\beta$), zero sideslip is quite accurately obtained by trimming the ball of the needle-ball instrument to the center, i.e., zeroing any lateral accelerations on the aircraft. If, however, the airplane has weak side force characteristics or has an asymmetric load or asymmetric thrust, an independent reference to give zero sideslip is required. A simple yaw string could be utilized and would be expected to put the airplane within ±1 deg of zero sideslip. As the subsequent error analysis shows, the error in initially obtaining zero sideslip acts much like a tare correction, and the calculated sideslip for most maneuvers will maintain the constant initial trim error in β. For the case where heading is maintained essentially constant, the β error will be equal to the initial zero β error times the cosine of the bank angle, and angle of attack will be in error by the magnitude of the initial zero β error times the sine of the bank angle.

26. Of course, a conventional sideslip vane on a nose-mounted boom could be utilized to give zero β. However, the use of IFP will obviate the need for boom mounted α and β vanes if another type of zero sideslip reference is utilized such as a yaw string.

BODY AXIS ACCELERATIONS

27. The acceleration of the aircraft with respect to the three aircraft body axes (A_x, A_y, A_z) was determined by differentiating the inertial velocities (V_N, V_E, V_V) and then transforming the resulting accelerations to the body referenced axis system. A "flat earth" assumption was made, and no attempt was made to compensate for the inertial system's torquing of its platform to keep itself aligned to true North and an earth-referenced vertical and to compensate for the coriolis effect. Because of the small magnitude of the resulting errors which occur at the airspeeds flown by a transonic aircraft, they can be ignored with negligible effect on the data. A more extensive discussion of these errors is presented in paragraphs 55 through 77. If desired, corrections for these effects can easily be made.

28. Inertial velocities were smoothed over five data bits using a third order least squares curve fitting routine. The derivative at the data point was then taken in order to calculate acceleration. In other words, the two velocity data bits prior to and the two after the data point were utilized for taking the derivative, i.e., a time span of 0.16 sec when data were computed at 25 times per sec. It was important to minimize the time span over which the data were smoothed to improve data accuracy during dynamic maneuvers.

FLIGHT PATH REFERENCED ACCELERATIONS

29. Acceleration along the aircraft's flight path was calculated by the following equation:

Acceleration Along the Flight Path (AFP):

$$AFP = A_x \cos\alpha + A_z \sin\alpha + A_y \sin\beta$$

30. In order to include the earth's gravity component and have parameters that are analogous to the outputs of accelerometers maintained normal to and along the flight path, the following equations were used:

Acceleration normal to the flight path (NZFP) - Units of g's:

$$NZFP = \frac{A_x \sin\alpha}{g} - \frac{A_z \cos\alpha}{g} + \cos\theta \cos\phi$$

Indicated Acceleration Along the Flight Path (AFPI) - Units of g's:

$$AFPI = \frac{AFP}{g} + \sin\gamma$$

31. Having less flight test value but useful for comparing IFP data with that from an accelerometer mounted along the aircraft's z axis is the conventional normal acceleration (N_z):

$$N_z = -\frac{A_z}{g} + \cos\theta \cos\phi$$

BODY AXIS ATTITUDE RATES AND ACCELERATIONS

32. The aircraft's attitude rates and attitude accelerations with respect to the aircraft body axis were determined by the following equations:

$$\dot{\phi} = d\phi/dt \qquad \dot{\theta} = d\theta/dt \qquad \dot{\psi} = d\psi/dt$$

$$p = \dot{\phi} - \dot{\psi} \sin\theta$$

$$q = \dot{\theta} \cos\phi + \dot{\psi} \cos\theta \sin\phi$$

$$r = \dot{\psi} \cos\theta \cos\phi - \dot{\theta} \sin\phi$$

33. $\dot{\theta}$, $\dot{\phi}$, and $\dot{\psi}$ were determined using the same third order curve fitting/differentiation routine utilized for determining body axes accelerations. In the same manner after p, q, and r were calculated, their derivatives were taken to yield pitch, roll, and yaw accelerations $\dot{p}$, $\dot{q}$, and $\dot{r}$.

INERTIAL MEASUREMENT UNIT LOCATION

34. If the inertial measurement unit (IMU) and C. G. are not collocated, the IMU will experience different accelerations than the C. G. of the aircraft. Fortunately, the IMU in the A-7C airplane is located within 6 in. (.15 m) of the C. G., and C. G. travel with fuel usage is minimal. Therefore, no compensation was made for the relative location of the IMU with respect to the C. G.

35. If the IMU were located at a position other than the C. G., the motion measured by the IMU can be transformed to motion about the C. G. The relative locations along the x, y, and z axes between the IMU and C. G. must be known. Appendix B presents the equations which can be utilized to transform IMU motion to aircraft C. G. motion, or in fact, the motion of any point on the airplane.

ACCURACY OF THE DATA

SOURCES OF ERRORS

36. The objectives of this section are to identify the primary IFP error sources and to show how each of these sources contributes to an error in the IFP data. The error sources in the IFP data can be categorized into four groups:

a. INS errors.

b. Air mass measurement errors.

c. Flat earth assumption errors.

d. Differentiation errors.

INS Errors

37. The technology of measuring the numerous errors of interest in inertial systems covers a wide range of specialty fields. In general, there are two opposing methods of measuring these errors. One is to make a sufficient number of measurements to statistically define the errors; the other is to use instrumentation with accuracy an order of magnitude better than the errors being measured. This last requirement challenges the accuracy of measurement standards (reference 4). Instead of actually attempting to measure the INS errors, the approach taken in this section is to show how a given error in an INS (attitude or acceleration) affects the INS output (velocity and position).

38. Two examples will be used to illustrate the relationship between the INS attitude and acceleration errors and the resultant navigation errors. It should be noted that the A-7C's INS navigates with a mean navigation error of less than 2 nmi/hr (3 700 m/hr).

EXAMPLE 1

39. A single axis INS is modeled as an accelerometer on a stabilized level platform (figure 4).

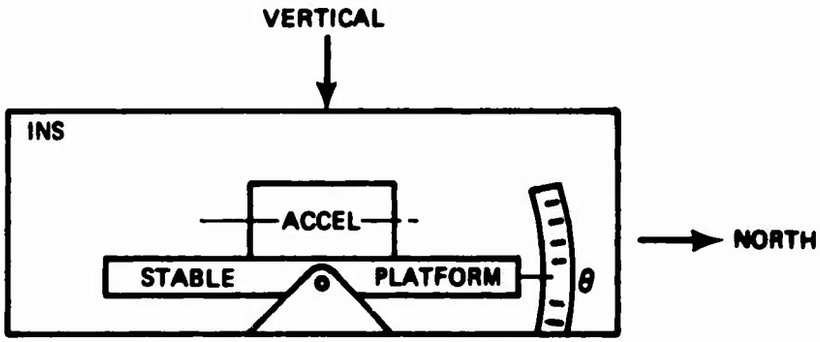

Figure 4
Example of Stabilized Platform

40. The above example is representative of the North axis of an INS with the Schuler feedback loop removed. It is assumed that the INS initial velocity is zero and the actual North acceleration of the INS is zero ($A_N = 0$). However, the accelerometer is assumed to have an acceleration measurement error of .001 g ($\Delta A_N = .001$ g). This accelerometer error will be interpreted erroneously as a true acceleration, and the INS will integrate the error as illustrated below.

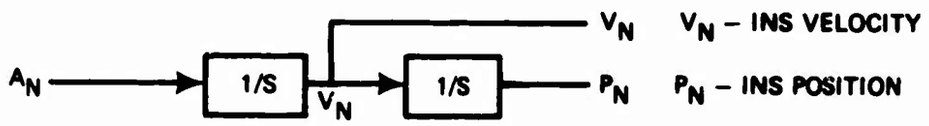

41. Figure 5 presents the INS velocity error (ΔV_N) and position error (ΔP_N) as the result of this .001 g error in acceleration measurement.

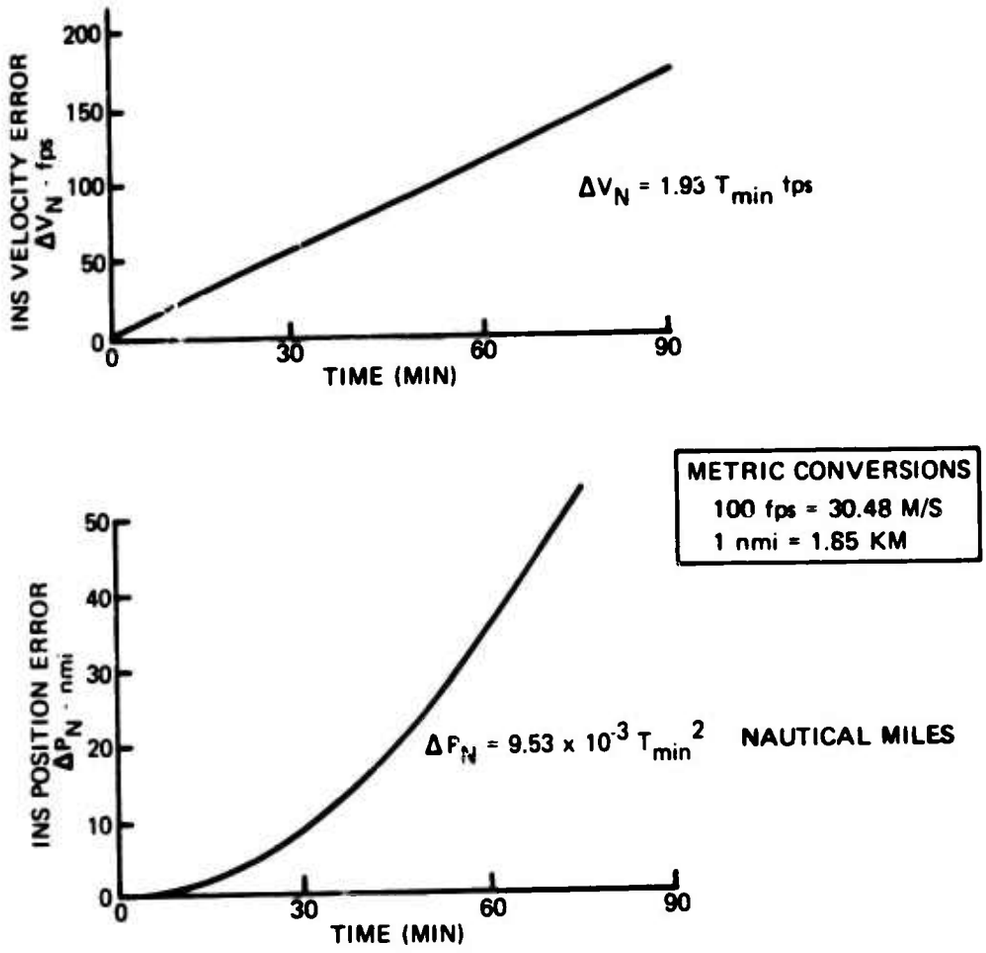

Figure 5
Simplified INS Errors

42. In the above example a .001 g accelerometer error caused velocity and navigation errors of 116 fps (35.4 m/s) and 34 nmi (63 km), respectively, after 1 hour. As will be shown subsequently, the short-term velocity error is of primary importance. The maximum velocity error change in a 2 minute period was only 3.86 fps (1.18 m/s) (or 3.3 percent of the total velocity error after 1 hour) despite the very large navigation error. If an attitude error occurred and the platform was not level (i.e., $\theta \neq 0$), the accelerometer would indicate an erroneous acceleration. An attitude error of +.0573 deg would cause the accelerometer to indicate an erroneous .001 g. The INS will interpret this signal as true acceleration to the North and consequently produce the same velocity and position errors as depicted in figure 5.

EXAMPLE 2

43. A more accurate model of the INS which includes the Schuler loop is illustrated below (figure 6).

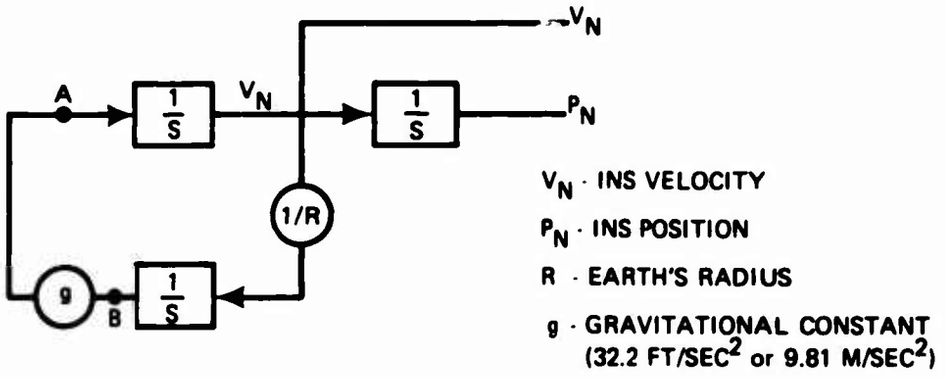

Figure 6
(Adapted from Reference 3)
Simplified INS Block Diagram

44. Again it is assumed that the INS initial velocity is zero and the actual acceleration of the INS is zero. A .001 g error in the accelerometer (acting at point A) or equivalently a .057 deg tilt error of the platform (point B) would cause identical INS velocity and position errors. Figure 7 presents the INS velocity and position errors resulting from the .001 g acceleration or .057 deg attitude errors.

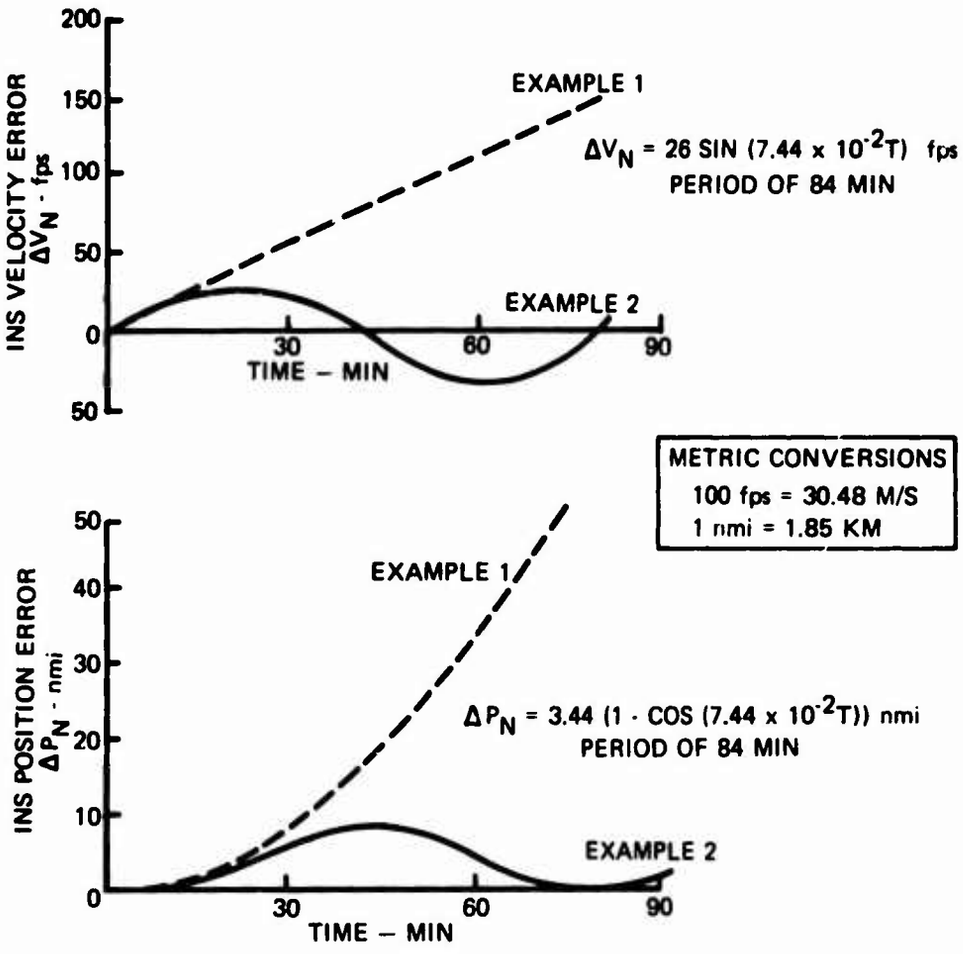

Figure 7
Simplified INS Error (with Schuler Loop)

45. The following errors are noted from figure 7.

a. A maximum position error (ΔP_N) of 6.9 nmi (12.8 km).

b. A maximum velocity error (ΔV_N) of 26 ft/sec (7.92 m/s).

c. A maximum "short-term" velocity error of 3.8 ft/sec (1.16 m/s).

46. The above examples illustrate that the navigation errors are very sensitive to acceleration and/or attitude errors. These two simplified examples of an INS should show that an INS that navigates with satisfactory accuracy (less than 2 nmi/hr or 3.7 km/hr) measures accelerations to accuracies of mili g's and attitudes to accuracies of arc minutes.

Air Mass Measurement Errors

47. The basic vector equation representing the navigation solution is

$$\bar{V}_A + \bar{V}_W = \bar{V}_I$$

Where $\bar{V}_A$ - velocity vector of the aircraft relative to the air mass

$\bar{V}_W$ - wind velocity vector (velocity of the air mass relative to the inertial frame)

$\bar{V}_I$ - velocity vector of the aircraft relative to the inertial frame.

Solving the above equation for $\bar{V}_W$ gives

$$\bar{V}_W = \bar{V}_I - \bar{V}_A \qquad \text{Equation A}$$

48. The above equation shows that the wind vector can be obtained by taking the difference between the air mass reference velocity ($\bar{V}_A$) and the inertial velocity ($\bar{V}_I$). This equation is mechanized in the A-7C's tactical computer. In order to investigate the effects of errors in $\bar{V}_A$ and $\bar{V}_I$ on the IFP data, the "measured" air mass velocity vector ($\hat{\bar{V}}_A$) and the measured inertial velocity vector ($\hat{\bar{V}}_I$) are defined as

$$\hat{\bar{V}}_I = \bar{V}_I + \Delta\bar{V}_I \qquad \text{Equation B}$$

and

$$\hat{\bar{V}}_A = \bar{V}_A + \Delta\bar{V}_A$$

49. The above equations illustrate that the measured velocities ($\bar{V}_I$ and $\bar{V}_A$) contain error vectors ($\Delta\bar{V}_I$, $\Delta\bar{V}_A$). Therefore, the wind vector computed from the "measured" inertial velocity and air mass velocity will also contain errors. That is, the computed or "measured" wind ($\bar{V}_W$) is

$$\hat{\bar{V}}_W = (\bar{V}_I + \Delta\bar{V}_I) - (\bar{V}_A - \Delta\bar{V}_A) \qquad \text{Equation C}$$

50. A comparison of the measured wind with the ideal wind equation (Equation A) shows that the wind error is

$$\Delta\bar{V}_W = \Delta\bar{V}_I + \Delta\bar{V}_A$$

51. For flight test work one is usually interested in determining an air mass referenced velocity ($\bar{V}_A$). The normal convention is to express the magnitude of the vector as the true airspeed (V_A). The direction of the vector relative to the body axis system is specified by the angle of attack (α) and the sideslip (β). The following development shows that the air mass velocity vector, computed from an inertial velocity vector and wind velocity vector, is not dependent on the constant portion of the inertial velocity error.

52. The wind vector was computed at the beginning of each maneuver with the airplane in stabilized flight. The computed air mass velocity is thus

$$\hat{\bar{V}}_A = \hat{\bar{V}}_I - \hat{\bar{V}}_W$$

Substituting Equations B and C into the above gives

$$\hat{\bar{V}}_A = \bar{V}_I + \Delta\bar{V}_I - \overbrace{\left[(\bar{V}_I + \Delta\bar{V}_I) - (\bar{V}_A - \Delta\bar{V}_A)\right]}^{\hat{\bar{V}}_W}$$

53. Since the wind is frozen at the beginning of many maneuvers (time = t_o), the air mass referenced velocity is subsequently computed from the measured inertial velocity and the "frozen" wind. Under these conditions, the "measured" air mass velocity at any time during the maneuver becomes

$$\hat{\bar{V}}_A = \bar{V}_I + \Delta\bar{V}_I - \overbrace{\left[\bar{V}_{I(t_o)} - \Delta\bar{V}_{I(t_o)} - (\bar{V}_{A(t_o)} - \Delta\bar{V}_{A(t_o)})\right]}^{\hat{\bar{V}}_{W(t_o)}}$$

54. An analysis of the above equation yields the following:

a. The inertial velocity error can be broken into two parts: a constant error portion and a time dependent error portion.

1. Computed air mass referenced velocity is unaffected by the constant portion of the inertial velocity errors (i.e., when $\Delta V_I = \Delta V_{I(t_o)}$).

2. Computed air mass referenced velocity is affected by changes in inertial velocity error during the maneuver. Therefore, $\Delta V_I - \Delta V_{I(t_o)}$ will introduce errors into the computation of air mass referenced velocity (V_A). However, this term, the short term inertial velocity error, was shown previously to be a very small error source.

b. The errors in the air mass velocity vector can be broken into three parts: a wind change during the maneuver, an ADC true airspeed measurement error, and the airplane not being in zero sideslip when the winds are frozen. These affect computed air mass referenced velocity as follows:

1. Any change in wind magnitude and direction during a maneuver when the winds are frozen will cause the computed air mass referenced velocities (V_x and V_y) to be in error according to the corresponding magnitude and direction of the wind change.

2. If the ADC incorrectly computes true airspeed, the computed wind will be in error by the magnitude of the ADC error (Note 1). The direction of this wind error will be equal to the reciprocal of the heading of the airplane.

3. If the airplane is not in zero sideslip when the winds are frozen, the wind computation will be in error. The wind error will have a magnitude equal to the sine of the sideslip angle multiplied by the true airspeed ($V_A \sin \beta$) and a direction perpendicular to the aircraft's true heading.

NOTE 1. The magnitude of the ADC error can be checked in flight by observing the winds during a 360 deg level turn. If the actual winds do not change and inertial velocity errors do not change, the change in the magnitude of the computed winds will be caused by an ADC error (one half of the observed wind change is the ADC error).

Flat Earth Assumption

55. The INS gives velocities and platform altitudes with respect to a North pointing local vertical (NPV) axis system. This axis system will therefore rotate and experience centrifugal acceleration as the result of the earth's rotation and the airplane's translation over the surface of the earth. The INS velocities and altitudes were treated as inertial quantities; that is, these quantities were differentiated to obtain acceleration and attitude rates. Strictly this is only valid if these quantities were obtained with respect to a nonrotating nonaccelerating (i.e., fixed, flat-earth) axis systems. The purpose of this section is to quantify the effects of this fixed flat earth assumption when used with a North pointing local vertical INS. The errors introduced by making a flat nonrotating earth assumption when using a NPV axis system can be visualized by the following discussion.

56. Round Earth - First, it is assumed that the earth is round (spherical) but still nonrotating. It is easy to visualize the following two effects because of the translation of the airplane over the surface of the earth.

a. Pitch Rate - Since a slight "pushover" is required to follow the curvature of the earth, the airplane will experience a small nose down pitch rate. This will occur at a constant indicated aircraft attitude ($\theta = 0$) with respect to the NPV axis system.

b. Vertical Acceleration - Because of this slight "pushover" the airplane will experience a small acceleration toward the center of the earth and as a result the load factor (NZFP) will be less than 1 g. This effect will occur even if the aircraft maintains a constant altitude and, therefore, zero indicated vertical acceleration (V_V) with respect to the NPV axis system.

57. Round Rotating Earth - Since the earth is rotating, the following effects occur:

a. Additional pitch, roll, and yaw rates (θ, ϕ, ψ) caused by the earth's rotation rate occur. These terms exist even with a constant indicated aircraft attitude (ϕ,θ ,ψ) when referenced to the NPV axis system.

b. Centrifugal acceleration acting orthogonal to the spin axis of the earth occurs. This acceleration has a North and Vertical component; however, it would not be evident by the indicated accelerations from the NPV axis system.

c. An additional Coriolis term is caused by the tangential (or Easterly) acceleration of the airplane because of the change in radial distance from the earth's axis of rotation (i.e., for an airplane in level flight the tangential velocity decreases as latitude is increased).

58. The above describes the errors that will be present when the velocities and attitudes from the NPV axis system are treated as if they came from a nonaccelerating, nonrotating axis system. However, the magnitude of these errors can be easily calculated.

Coriolis and Centrifugal Acceleration Effects

59. The Coriolis and centrifugal acceleration effects can be combined to produce equations that yield the magnitude of acceleration errors that result from making the flat, nonrotating earth assumption. The equations to calculate the North, East, and Vertical Acceleration Errors are:

$$A_N - A_N' = \Delta A_N = 2\,\Omega\, V_{EI} \sin (LAT)$$

$$A_E - A_E' = \Delta A_E = 2\,\Omega\, V_{VI} \cos (LAT) - 2\,\Omega\, V_{NI} \sin (LAT)$$

$$A_V - A_V' = \Delta A_V = -2\,\Omega\, V_{EI} \cos (LAT) - \Omega \times (\Omega \times R)$$

A_N = North Acceleration Referenced to Inertial Space

A_N' = North Acceleration Referenced to the NPV

A_E = East Acceleration Referenced to Inertial Space

A_E' = East Acceleration Referenced to the NPV

A_V = Vertical Acceleration Referenced to Inertial Space

A_V' = Vertical Acceleration Referenced to the NPV

Ω = Earth's Rotation Rate (7.29×10^{-5} rad/sec)

LAT = Geodetic Latitude

X = Cross Product

60. The following "trends" can be derived from the above equations.

a. Most of the error terms are proportional to the airplane's inertial velocity and, in general, the error will be the largest for an airplane at high speeds.

b. Latitude (LAT) and the airplane's heading (ψ) are very influential factors.

61. The following examples illustrate the errors for an airplane at a true airspeed of 661 KTAS (1 224 km/hr) or Mach 1.0 at sea level.

a. North Acceleration Error - The largest North acceleration errors will occur at high speeds with the airplane on an Easterly heading at high latitudes. For example, when heading East at Mach 1 at 40 deg North latitude, the North acceleration error would be

ΔA_N = .003 g

b. East Acceleration Error - The largest East acceleration error (ΔA_E) will occur at high speeds at

Low latitudes with the airplane in a vertical dive ($\gamma = 90^o$). For example, at the Equator with the airplane in a Mach 1.0 vertical dive, ΔA_E = .005 g.

or

High latitudes with the airplane heading North. For example, when heading North at Mach 1 at 40 deg North latitude, ΔA_E = .003 g.

c. Vertical Acceleration Error - The Vertical Acceleration Error (ΔA_V) will be largest when the airplane is heading East at low latitudes. For example, at the Equator when heading East at Mach 1.0, ΔA_V = .0085 g.

62. In summary, it was shown that errors occur when the fixed flat earth assumptions are applied to a NPV referenced axis system. For a subsonic airplane, the maximum error introduced will be .0085 g.

63. The errors discussed in this section were considered acceptable for this application; however, they may be appreciable for other applications, e.g., high speed at critical latitudes. The correction terms discussed herein can be implemented easily in the software program, and USNTPS will compensate for these errors in its next iteration in IFP development.

64. The following block diagram (figure 8) illustrates how the acceleration corrections (ΔA_N, ΔA_E, ΔA_V) can be converted to corresponding body referenced acceleration corrections (ΔA_x, ΔA_y, ΔA_z). These correction terms would be added to the previously computed body referenced accelerations (paragraphs 27 through 31) to get the corrected A_x, A_y, and A_z.

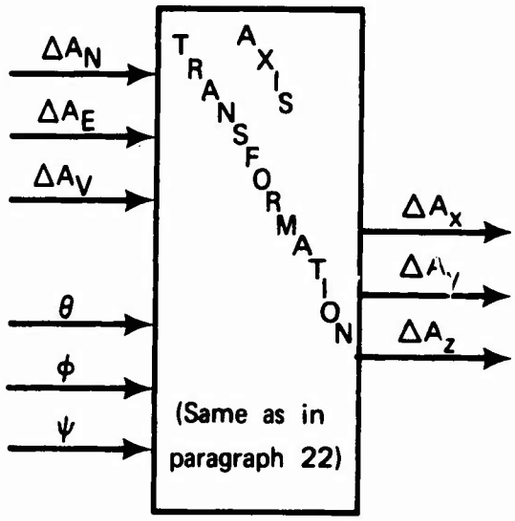

Figure 8
Acceleration Correction Block Diagram

Attitude Rate Effects

65. The platform attitudes (ψ, ϕ, θ) are measured with respect to the NPV axis system. As previously discussed, this axis system has a rotation rate caused by the earth's rotation rate and the aircraft's translation over the surface of the earth. The differences between attitude rates ($\dot{\theta}, \dot{\phi}, \dot{\psi}$) measured with respect to the NPV axis system and the "true" attitude rates are:

$$\Delta\dot{\theta} \doteq -\Omega \cos (\text{LAT}) \sin \psi - \frac{1}{R} (V_{NI}^2 + V_{EI}^2)^{1/2}$$

$$\Delta\dot{\phi} \doteq \Omega \cos (\text{LAT}) \cos \psi \cos \theta + \Omega \sin (\text{LAT}) \sin \theta$$

$$\Delta\dot{\psi} \doteq \Omega \sin (\text{LAT})$$

66. The magnitude of the pitch rate error is illustrated by the following example: An airplane is at the Equator heading East at 600 KTAS (949 km/hr) with $\theta = 0^{\circ}$. If the airplane remains at the above conditions ($\dot{\theta} = 0$), the attitude rate ($\dot{\theta}$), as indicated by the NPV data, will be zero. However, the inertially referenced pitch rate will not be zero. The inertially referenced pitch rate will be -.0042 deg/s (nose down) because the earth's rotation rate plus -.0028 deg/s because of the aircraft's translation over the earth's surface. Thus, a total pitch rate error of .007 deg/s would occur.

67. The above example represents a worst case condition (i.e., the earth's rotational term and the aircraft's translational term are additive). The translation effect will be greater at higher true airspeeds, and obviously the combination of earth rotation and aircraft translation will be lower when heading West. However, for current aircraft, this term may be neglected.

Differentiation Errors

68. The differentiation of the INS inertial velocities (V_{NI}, V_{EI}, V_{VI}) and attitudes (ψ, θ, ϕ) was required to get the IFP data (i.e., NZFP, p, q, r, etc). In general, the errors introduced by a smoothing/differentiation routine will be determined by:

a. The error power spectral density of the quantities being differentiated.

b. The effective bandwidth produced by the smoothing routine and the sample rate.

It is usually desirable to use the highest possible bandwidth; however, the high frequency noise and maximum sample rate will limit the bandwidth.

69. The "raw" inertial velocities and attitudes have very low noise levels, and therefore a relatively high bandwidth smoothing routine was used (3 deg polynomial through 5 data points). This routine gives an approximately bandwidth of 30 rad/sec with the sample rate of 25/sec and produces low noise levels (Appendix C).

70. The apparent noise level exhibited by the IFP data is low. The noise, however, appears to be concentrated at high frequencies which should not adversely affect normal airplane stability and control work. Lower noise levels may be obtained by increasing the smoothing (decreasing the bandwidth) if a lower bandwidth is permissible.

ERROR SENSITIVITY ANALYSIS

71. The previous section described the sources of errors in the IFP data. The purpose of this section is to quantify the effects of various INS and air mass errors on the IFP data. In order to determine how an error affects the IFP data, one can trace the error through the various transformations that were used to calculate each inertially derived parameter (paragraphs 20 through 33). Having done this, one can show the sensitivity of each inertially derived flying quality and performance parameter to each error source.

72. The procedure for determining the sensitivity of an inertially derived parameter to an error source is in concept simple. For example, to determine what angle of attack error ($\Delta\alpha$) would be caused per unit of INS velocity error (ΔV_I), one can perturbate the inertial velocity (V_I) by the assumed error (ΔV_I) and then compute the resultant change in the computed angle of attack (α). The sensitivity term is then:

$$\frac{\partial \alpha}{\partial V_I} \doteq \frac{\Delta \alpha}{\Delta V_I}$$

The angle of attack error is therefore

$$\Delta\alpha = \left(\frac{\partial \alpha}{\partial V_I}\right) \Delta V_I$$

73. The sensitivities of the IFP variables to the primary sources of errors were computed for various flight conditions (V_A, ϕ, θ, ψ). Table II summarizes the results of this sensitivity analysis.

Table II

IFP Error Sensitivities

IFP Variable	Primary Error Sources	Sensitivity (Note 2)	Flight Condition to Maximize Error (i.e., Maximum Sensitivity)
	Erroneous INS Velocity Change During Maneuver	$\frac{\Delta \gamma}{\Delta V_I} \doteq \frac{57.3}{V_A} \frac{\text{deg}}{\text{kt}}$ *	Total INS velocity error (ΔV_I) is orthogonal to the airplane's velocity vector and the airplane's y axis.
	Wind Change During Maneuver	$\frac{\Delta \gamma}{\Delta V_W} \doteq \frac{57.3}{V_A} \frac{\text{deg}}{\text{kt}}$ *	Total wind vector error (ΔV_W) is orthogonal to the airplane's velocity vector and the airplane's y axis.
	Sideslip Error at Wind Freeze	$\frac{\Delta \gamma}{\Delta \beta} \doteq \sin \phi \cos \phi$ in deg/kt	Airplane remains on same heading and changes bank angle by 90° after wind is frozen (Note 1).
	ADC Error at Wind Freeze	$\frac{\Delta \gamma}{\Delta V_{AC}} \doteq \frac{57.3 \sin \phi \sin \theta}{V_A}$ in deg/kt	Airplane changes bank angle and heading by 90° after wind is frozen (Note 1)
	Erroneous INS Velocity Change During Maneuver	$\frac{\Delta \theta}{\Delta V_I} \doteq \frac{57.3}{V_A} \frac{\text{deg}}{\text{kt}}$ *	INS velocity error vector (ΔV_I) occurs along airplane's y axis.
	Wind Change During Maneuver	$\frac{\Delta \theta}{\Delta V_W} \doteq \frac{57.3}{V_A} \frac{\text{deg}}{\text{kt}}$ *	Total wind vector error (ΔV_W) along airplane's y axis.
	Sideslip Error at Wind Freeze	$\frac{\Delta \theta}{\Delta \beta} \doteq \cos \phi \cos \theta$ in deg/deg	Airplane remains at same nominal pitch and roll angle after wind is frozen (Note 1).
	ADC Error at Wind Freeze	$\frac{\Delta \theta}{\Delta V_{AC}} \doteq \frac{57.3}{V_A}$ in deg/kt *	Airplane makes 90° heading change after freezing winds (Note 1).
AFPI	Angle of Attack Error	$\frac{\Delta AFPI}{\Delta \alpha} \doteq \frac{NZFP}{57.3}$ in g/deg	Large value of airplane acceleration normal to flight path.
NZFP	Angle of Attack Error	$\frac{\Delta NZFP}{\Delta \alpha} \doteq \frac{AFPI}{57.3}$ in g/deg	Large value of airplane longitudinal acceleration.
P_s	ADC Error at Wind Freeze	$\frac{\Delta P_s}{\Delta V_{AC}} \doteq 1.69$ AFPI in ft/sec/kt	Large value of airplane longitudinal acceleration.
	Wind Change After Freezing Wind	$\frac{\Delta P_s}{\Delta V_W} \doteq 1.69$ NZFP * in ft/sec/kt	Total wind vector error orthogonal to flight path and airplane's y axis.
	Erroneous INS Velocity Change During Maneuver	$\frac{\Delta P_s}{\Delta V_I} \doteq 1.69$ NZFP * in ft/sec/kt	Short term INS velocity vector error orthogonal to flight path and airplane's y axis.
	Angle of Attack Error	$\frac{\Delta P_s}{\Delta \alpha} \doteq \frac{1.69}{57.3}$ NZFP V_{AC} in ft/sec/deg	Large value of airplane acceleration normal to flight path and high true airspeed.

* Worst case sensitivity, i.e., the error vector acting orthogonal to or along a particular axis.

NOTES 1. The winds are frozen with $\phi = 0$ and $\theta = 0$.
2. The units of all velocities (V_A, V_W, etc.) should be in knots.

74. In order to keep table II to a manageable size, it does not present the sensitivity of each inertially derived parameter to every error source but rather only the significant error sources. Many inertially derived parameters were omitted from table II since their error sensitivities are obvious. For example, the magnitude of A_x, A_y, and A_z errors will have a direct correlation (i.e., through the transformations) with the magnitudes of A_N, A_E, and A_V errors. In the same sense, the magnitudes of V_x, V_y, and V_z errors have a direct correlation with the magnitudes of V_N, V_E, and V_V errors.

75. Table II shows that α and β errors caused by erroneous inertial velocity changes and wind errors during a maneuver are inversely proportional to the true airspeed. For example, at 300 KTAS (556 km/hr) the worst case α and β sensitivities to short term INS and wind errors are 0.2 deg/kt (.39 deg/m/s). At 600 KTAS (1 111 km/hr) the worst case error sensitivity is 0.1 deg/kt (0.19 deg/m/s).

76. Table II shows that P_s is very sensitive to short term inertial velocity errors, wind vector errors, and angle of attack errors. These sensitivities are directly proportional to acceleration normal to the flight path.

77. An analysis of the error sensitivities shows that certain maneuvers can be performed which will maximize an inertially derived parameter's error. Conversely, maneuvers can be selected to minimize errors in the parameters of interest. For example, with an ADC error (ΔV_{AC}), the angle of attack errors will be minimized by conducting maneuvers on approximately the same heading as existed when the wind was frozen.

FLYING QUALITIES DATA

78. Since the on-board computer sample rate of all inertial parameters was 25 times per sec, the IFP system was very effective for stability and control testing. At this sample rate, aircraft frequency response up to 30 rad/sec (approximately five cycles/sec) could be adequately documented. This frequency response capability should be adequate for most aircraft stability and control applications and is well within the 20 cycle/sec frequency response capability of the INS.

79. A random sample of curves showing typical stability and control test maneuvers is presented in Appendix C. The data are consistent with previously obtained A-7 stability and control data and the cockpit data taken during the test flights. Of note is that each of these curves was plotted from the raw unfiltered IFP data. As previously mentioned, neither cockpit control force nor control surface position data were available during this feasibility study and consequently are not depicted on any of the curves presented herein.

80. A data sample rate of fives times per sec appears adequate for some stability and control testing such as dutch roll characteristics (Appendix C, figures 1 through 4). However, the 25 times per sec sample rate is required for documenting the typically higher frequency modes of motion such as the airplane's short period response and roll performance. Appendix C, figures 5 through 12, give comparisons of the same short period maneuver when plotted at fives times and 25 times per sec. The improved quality of the data at higher sample rate is apparent.

81. Acceleration sensitivity, or the variation of normal acceleration with angle of attack, was determined by plotting acceleration normal to the flight path (NZFP) versus α. Appendix C, figures 11, 12, and 13, show NZFP as a function of α during a short period excitation maneuver and during a maneuvering stability wind-up turn.

82. Appendix C, figures 14 through 23, present time histories of the A-7C airplane's roll performance at 200 KIAS (103 m/s) and 400 KIAS (206 m/s). The roll rates and the magnitudes and direction of the sideslip during these roll tests were consistent with cockpit data and available A-7 stability and control data.

83. A review of Appendix C shows that all parameters are essentially noise free. A comparison of Appendix C, figures 17, 18, 22, and 23, show the significant improvement in the quality of the angle of attack measurement when the inertially derived α vice the airplane's production vane α is utilized. The noise on the vane α curves appears to be exacerbated when dynamic pressure and/or angle of attack is increased, which is probably a result of angle of attack vane flutter.

PERFORMANCE DATA

84. The phase of flight testing to which IFP provides the most apparent benefits is aircraft performance testing. A data sample rate of five times per sec was used and found to be adequate for the performance testing maneuvers conducted during this program.

TAKEOFF AND LANDING PERFORMANCE

85. Takeoff distances can be determined by integrating velocity from the start of the takeoff roll until weight-off-gear or until vertical velocity starts to increase. Similarly landing distances can be determined by integrating velocity from touchdown (weight-on-gear and/or vertical velocity going to zero) until the airplane stops. If the inertial system has residual velocities at the time of these tests, the data can easily be corrected for the known zero velocity which exists at the beginning of the takeoff roll and at the end of the landing roll. Using the IFP system for takeoff and landing performance tests obviates the need for external camera coverage for these tests.

SPECIFIC EXCESS POWER

86. Specific excess power (P_s) is determined with conventional instrumentation by taking the derivatives of pitot-static derived energy height (E_h) as follows:

h = altitude

g = 32.2 ft/sec^2 (9.81 m/sec^2)

v = true airspeed (ft/sec)

γ = flight path angle

$$E_h = h + \frac{v^2}{2g}$$

$$\frac{dE_h}{dt} = \frac{dh}{dt} + \frac{v}{g}\frac{dv}{dt}$$

$$\frac{dE_h}{dt} = P_s = \frac{dh}{dt} + \frac{v}{g}\frac{dv}{dt}$$

87. Level flight acceleration runs are typically conducted for this purpose. With the IFP system, P_s can be determined in another way.

$$P_s = \frac{dh}{dt} + \frac{v}{g}\frac{dv}{dt}$$

$$\frac{P_s}{V} = \frac{1}{v}\frac{dh}{dt} + \frac{1}{g}\frac{dv}{dt}$$

and since $\frac{1}{v}\frac{dh}{dt} = \sin\gamma$

and $\frac{dv}{dt}$ = AFP (acceleration along the flight path)

$$\frac{P_s}{v} = \sin\gamma + \frac{AFP}{g}$$

and $\sin\gamma + \frac{AFP}{g}$ = AFPI as defined in paragraph 30.

Therefore, $P_s = V \cdot AFPI$.

88. With this relationship, P_s was available during every test maneuver by multiplying indicated acceleration along the flight path (AFPI) by true airspeed.

89. A level flight acceleration run was conducted, and Appendix C, figure 24, shows a comparison of P_s derived by the conventional pitot-static method and P_s derived by the IFP system. The data show good agreement over the entire airspeed range; however, the P_s derived by the IFP system appears to have considerable noise. An examination of Appendix C, figure 25, which is a curve of acceleration normal to the flight path (NZFP) versus true airspeed (V_A) during this same acceleration run, shows a high degree of correlation between NZFP and the P_s derived by the IFP system. That is, when the NZFP shows a peak g greater than one, the P_s curve shows an associated "dip" to a local minimum. This feature of the data is exactly what one would expect (i.e., as g increases, the airplane drag increases and thus P_s decreases). This is an example of how the accuracy and dynamic response capability of the IFP system show features in the data not previously discernible.

90. Appendix C, figure 26, is a plot of inertially derived angle of attack versus vane angle of attack during this same acceleration run. The data show good correlation at the low angles of attack. The nominal 1.5 deg difference between the angle of attack values from each source is probably the result of the angle of attack vane being boresighted to a different fuselage reference line. No further flights were conducted to confirm this hypothesis, but additional testing is recommended to develop further confidence in the absolute values of inertially derived angles of attack.

MANEUVERING PERFORMANCE

91. A constant airspeed wind-up turn was conducted, and the variation of P_s as a function of $(NZFP)^2$ is presented in Appendix C, figure 27. As expected, the variation of P_s with $(NZFP)^2$ is linear at the low g levels and then, at the higher g levels, decreases more rapidly with $(NZFP)^2$. With this one maneuver, the P_s characteristics of the test airplane were completely documented for the given altitude and airspeed. From these data the following were determined:

a. The level flight P_s (P_s = 67.5 ft/sec (20.6 m/s) at NZFP = 1.0) which is usually obtained from level acceleration runs.

b. The sustained g capability of the airplane (NZFP = 2.59 g) which is usually obtained from level turn performance tests.

c. The "high" g P_s values (e.g., P_s = 25,000 FPM (127 m/s) at 5 g's) which are not available from conventional flight testing. Conventional methods of determining P_s at different g levels require knowledge of the airplane's drag polars.

DYNAMIC PERFORMANCE TESTING

92. The purpose of dynamic performance testing is to obtain aircraft performance information from dynamic maneuvers rather than from time-consuming, and therefore, expensive, steady-state test maneuvers. It has been estimated that a 70 to 90 percent savings in flight time could be realized by application of the dynamic performance method in an extensive performance program (reference 5).

93. The basis of dynamic performance testing is the accurate determination of flight path referenced accelerations (i.e., normal to and along the airplane's flight path). With conventional dynamic performance methods, special acceleration packages are used to measure the accelerations with respect to the airplane's body axes. These accelerations are then transformed to the flight path axis via boom measured angle of attack (α_B) and sideslip (β_B). These boom measured quantities (α_B, β_B) are subject to various errors. The error sources and the causes of each are listed in table III.

Table III

Error Sources for Boom Measured Angle of Attack and Sideslip

Error Source	Causes
Boom Bending Errors	$\alpha_E = f(n_z, \dot{q}, Q, \alpha, M)$
	$\beta_E = f(AYI, \dot{r}, Q, \beta, M)$
Interference Errors	$\alpha_E = f(\alpha, \beta, M)$
	$\beta_E = f(\alpha, \beta, M)$
Dynamic Errors	$\alpha_E = f(q)$
	$\beta_E = f(r)$

94. As illustrated in table III, many of the causes of errors are "dynamic" in nature (e.g., n_z, θ, q, r). Approximate corrections are applied for some of these effects (reference 5), but significant residual errors still occur. Since the more "dynamic" maneuvers produce larger errors, the error sources become a limiting factor for the maneuvers and therefore limit the potential of the dynamic performance method.

95. The inertially derived α and β are very accurate under dynamic conditions. It was shown previously that the primary error sources for the IFP data are not rate dependent. In fact, some of the primary error terms are minimized if the maneuver is completed in a short period of time. These characteristics of the INS derived α and β will enhance the dynamic performance method by removing some of the instrumentation imposed restrictions on the flight test maneuvers. This should increase the efficiency (amount of data per unit flight time) of the dynamic performance testing method. Additionally, the use of a proven, highly accurate INS will remove the need for the extensive calibration required with a conventional dynamic performance package which sometimes involves calibrating the accelerometers before and after each data flight.

NEW OR IMPROVED CAPABILITIES FOR FLIGHT TESTING

96. Besides providing more accurate data than was previously obtainable, IFP offers additional and improved flight test capabilities. Many of these new capabilities obviate the need for external data gathering sources and therefore provide significant cost and time savings to the flight test team.

97. As described previously, takeoff and landing distances can be determined by integrating velocity during the takeoff roll and landing roll. This eliminates the need for external camera coverage to measure takeoff and landing distances.

98. Many aircraft carrier suitability tests can be performed using solely the IFP instrumentation system as the data source. Altitude lost during catapult minimum end airspeed determinations can be determined by integrating vertical velocity after the catapult launch, whereas previously the "Mod one eyeball" of the carrier suitability engineer when combined with the calibrated "seat of the pants" feel of the test pilot was utilized to determine sink off the bow. (Historically, camera coverage produced inaccurate altitude lost results.)

99. In carrier suitability testing postcatapult launch longitudinal acceleration, expressed as a/g (longitudinal acceleration divided by gravity), must be greater than 0.04 (reference 6). Previously, the value of a/g had to be calculated from thrust required and thrust available data (i.e., a/g = (T-D)/W), and the actual postcatapult launch a/g was never directly measured. IFP will finally give the carrier suitability test team the capability to measure a/g directly even during the very dynamic catapult launch evolution.

100. The altitude lost during a wave-off has been determined traditionally at NATC by using SPN-42 radar tracking. With IFP the same degree of data accuracy during this test should be available without the use of the external radar.

101. Carrier suitability structural landing demonstrations are still plagued in not being able to measure with repeatable accuracy aircraft landing sink speed and aircraft touchdown attitude. Camera coverage, doppler radar, and TRODI (touchdown rate of descent indicator) mirrors have all been tried, but none have proven to have the desired repeatable accuracy. IFP offers another alternative which should prove more accurate than any previous method and it requires no external tracking device. Since IFP lends itself well to telemetry, real-time data processing could obviously be used for these tests.

102. Static source position error determinations at normal accelerations other than one and during transonic flight are possible from using the IFP system. IFP will not replace traditional methods for airspeed calibration at one "g," but IFP offers a method of calibrating static source position error during accelerated flight which was never previously possible. This should be quite valuable in the development of software for an air-to-ground weapon system that uses barometric inputs in its weapons delivery computations.

103. As discussed in the Performance Section, IFP is an outstanding system for dynamic performance testing. Having a continuous readout of specific excess power (P_s) gives the flight test team new methods to obtain performance data and enables them to directly obtain performance comparisons that previously required the knowledge of the aircraft's drag polars (e.g., plotting P_s at different g levels).

104. A constant Mach wind-up turn or a constant g acceleration run can be conducted to determine P_s as a function of airspeed and normal acceleration. This will obviate the need for having the test pilot conduct the traditional stabilized point level turn performance tests. (The g at which P_s equals zero is the level flight sustained turn performance at each specific airspeed.)

105. Having accurate P_s data available at various g levels will enable the flight test team to better compare the aircraft's actual performance with its design criteria. It will also give the requirements determination people the opportunity to measure actual maneuvering performance in current aircraft against potential threats and to more accurately quantify the performance needs of future aircraft to successfully engage potential threats. The operational requirements people will have the capability of more completely defining a needed performance envelope, and the testers will be better able to document each aircraft's total performance envelope.

106. Since IFP continuously calculates flight path angle, (γ), an aircraft's open loop vertical height response to control inputs can be accurately documented (i.e., Bode plots can be made of longitudinal control input frequency to output gain). This capability should permit easier derivation of the software to be used in automatic control such as for automatic carrier landings.

107. Because of the high accuracy and low noise of IFP data, it should be extremely valuable in parameter identification work (Note 1). Flying quality parameters which have shown themselves as being noisy in their application to parameter identification are: airspeed, pitch, roll, and yaw accelerations; normal acceleration; and longitudinal acceleration. Pitch, roll, and yaw accelerations are particularly difficult to obtain, and three axes angular rate measurement devices are currently being developed for this purpose. IFP, however, produces the accurate, low-noise determination of all the necessary aircraft motion parameters for parameter identification work. It is recommended that a determination of IFP data consistency for parameter identification work be conducted such as by using an optimum filtering/smoothing routine.

NOTE 1. Parameter identification or parameter estimation are the methods used in system identification problems. In aircraft flight testing this technique has traditionally referred to the determination of stability and control derivatives. The technique involves the estimation of the characteristics (e.g., stability derivatives) from input/output measurements. Usually the set of equations that describe the response being observed is known, and parameter identification is used to estimate the value of each term in the set of equations.

COST COMPARISON

108. An instrumentation system employing the IFP concept offers a significant cost savings, especially if the aircraft being tested has an INS. If an onboard INS is not available, the relatively high cost of an INS may dissuade many potential users from employing IFP.

109. Since rate gyros, accelerometers, attitude sensors, a boom with angle of attack and sideslip vanes, and the associated signal conditioning is not required if IFP is utilized, the attendant cost savings are obvious. Since these items do not have to be installed, maintained, or calibrated, there is also a significant savings in the labor requirements to install, maintain, and calibrate an IFP instrumentation system.

110. A nominal 150 man days of labor is being saved in installation labor at TPS by utilizing IFP in an A-7C. This number was obtained by comparing the IFP instrumentation installation labor requirements with the labor requirements for fully instrumenting a fixed wing airplane for FQ&P testing at TPS using conventional instrumentation. This is not a very good comparison since the IFP instrumentation system will have significant additional instrumentation capabilities which previously have not been utilized at TPS (i.e., those additional instrumentation parameters required for dynamic performance testing, e.g., flight path accelerometers).

111. With IFP no requirement exists to know the relative magnitudes of each of the parameters to be recorded prior to the flight. Therefore, instrumentation preflight time is reduced since the instrumentation parameter sensitivities (expected peak to peak values of each parameter) do not have to be set up according to the type of flight being flown.

112. An IFP system enables the test aircraft to use its on-board instrumentation system to determine quantities which historically have been determined by use of external sensors. Examples discussed previously include: takeoff and landing distances, wave-off altitude loss, structural landing tests requiring touchdown attitudes and sink speed, altitude lost during catapult minimum end airspeed tests aboard ship, open loop aircraft vertical height response for automatic control testing, and transonic static system position error determination. Since external cameras, radar tracking, or chase aircraft are not required for the previously listed tests, the cost savings thereby accrued are a result of IFP instrumentation.

CONCLUSIONS

GENERAL

113. An inertial system can be successfully used to derive the conventional parameters which describe the motion of an aircraft. This method of instrumentation offers significant advantages over conventional methods of instrumentation.

SPECIFIC

114. Traditional flying qualities and performance data were easily obtained with higher accuracy and less noise than conventional instrumentation systems (paragraphs 78 through 89).

115. A boom for angle of attack and sideslip vanes was not required to obtain these parameters. The accuracy of these parameters (especially during dynamic maneuvers) from the IFP system was greatly improved over conventionally obtained angle of attack and sideslip (paragraphs 26 and 95).

116. If an inertial system is already available in the test aircraft, a significant cost savings can be accrued from IFP (paragraphs 108 through 112).

117. External data coverage is not required for many tests that previously required camera or radar tracking (paragraphs 85, 100, and 101).

118. New test capabilities are available with IFP such as specific excess power determination during any maneuver and static source position error determination at normal accelerations other than one (paragraphs 96 through 106).

119. The data are of the quality that make them highly useful for dynamic performance testing and flying quality parameter identification work (paragraphs 95 and 107).

120. If an aircraft has an INS that determines North, East, and Vertical Velocities and aircraft attitude; and ADC that calculates true airspeed; and a recording device for these parameters, the aircraft processes a full IFP package which is compatible with NATC software to calculate: α, β, γ, p, q, r, $\dot{p}$, $\dot{q}$, $\dot{r}$, A_x, A_y, A_z, n_z, p_s, etc. (paragraphs 20 through 33).

121. Disadvantages of IFP instrumentation include:

a. Accurate air mass referenced airspeed is required (paragraphs 21 and 47).

b. An independent method of determining zero sideslip is required (paragraphs 25 and 26).

c. If the wind changes during a test maneuver, the data will have errors (paragraph 54).

d. Presently, there is no compensation for the vertical component of wind (paragraph 21).

e. High cost of purchasing an INS (paragraph 108).

122. Additional advantages of IFP instrumentation include:

a. Shorter instrumentation installation time (paragraph 110).

b. Lower instrumentation installation cost (paragraph 109).

c. Reduction in instrumentation maintenance (paragraph 109).

d. Calibrations of attitude, acceleration, and rate sensors are not required (paragraphs 95 and 109).

RECOMMENDATIONS

123. More fully utilize the capabilities of an aircraft's inertial system for FQ&P testing.

124. Investigate the development of a portable IFP system.

125. Determine IFP data consistency for parameter identification work (paragraphs 90 and 107).

REFERENCES

1. Olhausen, J. N., "The Use of a Navigation Platform for Performance Instrumentation on the YF-16 Flight Test Program," AIAA Paper 75-32, presented in Pasadena, California, Jan 1975.

2. Wagner, F., Cargill, L. B., Murphy, R. C., and Phillips, F. A., Avionics and Armament Service Acceptance Trials of the A-7E Airplane, NATC Technical Report WST-017R-70, of 27 Feb 1970.

3. McRuer, D., Ashkenas, I., and Graham, D., Aircraft Dynamics and Automatic Control, Princeton University Press, Princeton, New Jersey, 1973.

4. Merrill, G., Principles of Guided Missile Design, D. Van Nostrand, Company, Princeton, New Jersey, of 1962.

5. Pueschel, P., Development of Dynamic Methods of Performance Flight Testing, Report No. ADR 07-01-70.1, Grumman Aerospace Corporation, New York, Aug 1970.

6. Bowes, W. C. and Stento, L. V., "Catapult Launch Minimum End Airspeed Tests," Pilots Handbook for Critical and Exploratory Flight Testing, Society of Experimental Test Pilots, Lancaster, California, and AIAA, New York, 1972.

TRANSFORMATION OF IMU MOTION TO C. G. MOTION

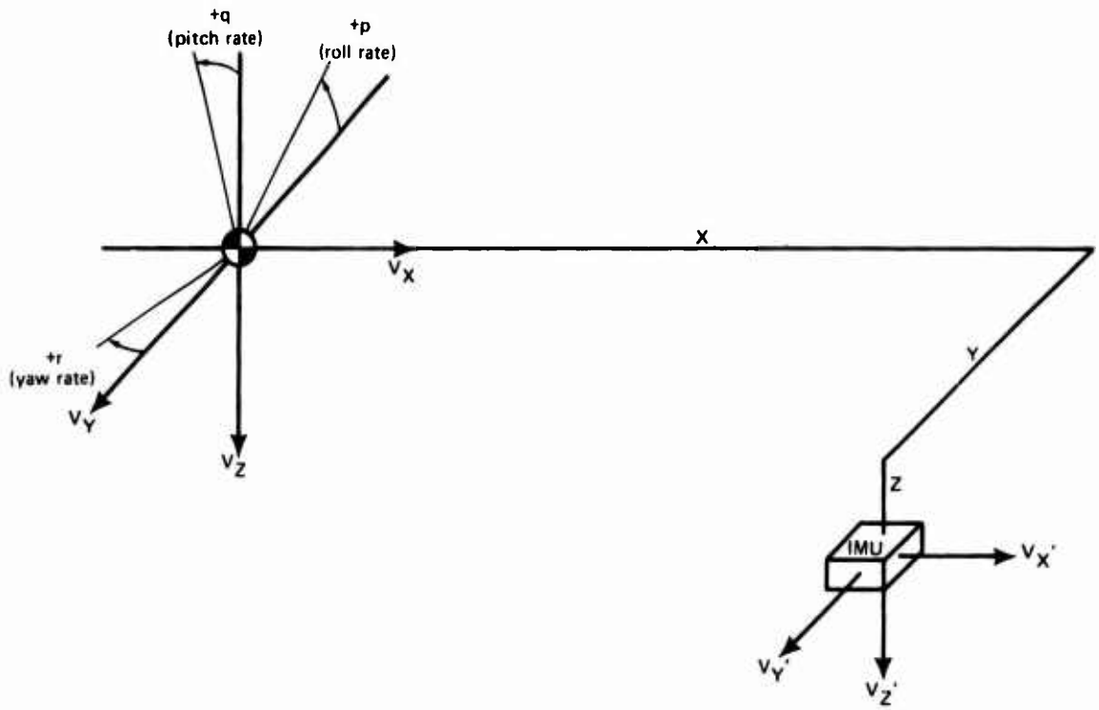

V_x	C. G. velocity along x axis
V_y	C. G. velocity along y axis
V_z	C. G. velocity along z axis
V_x'	IMU sensed velocity along x axis
V_y'	IMU sensed velocity along y axis
V_z'	IMU sensed velocity along z axis
x	distance from C. G. to IMU along x axis of aircraft
y	distance from C. G. to IMU along y axis of aircraft
z	distance from C. G. to IMU along z axis of aircraft

p, q, r	true angular rates of aircraft about C. G.
$\Delta V_x, \Delta V_y, \Delta V_z$	increments in sensed body axes velocities at the IMU because of aircraft rotation
$\Delta A_x, \Delta A_y, \Delta A_z$	increments in sensed body axes accelerations at the IMU because of aircraft rotation

$$\Delta V_x = y r - z q$$

$$\Delta V_y = z p - x r$$

$$\Delta V_z = x q - y p$$

$$\Delta A_x = y \dot{r} - z \dot{q} + x (q^2 + r^2) - p (y q + z r)$$

$$\Delta A_y = z \dot{p} - x \dot{r} + y (p^2 + r^2) - q (z r + x p)$$

$$\Delta A_z = x \dot{q} - y \dot{p} + z (p^2 + q^2) - r (x p + y q)$$

Assuming no bending and a rigidly mounted IMU, the attitude rates and attitude accelerations of the IMU will be identical to those of the C. G. regardless of IMU location on the aircraft. If the INS gives a velocity output, accelerations are determined by differentiating velocity along each axis. Therefore, only V_x, V_y, and V_z need to be corrected if the IMU and C. G. are not collocated.

In order to correct the IFP derived velocities about the IMU to velocities about the C. G., the increments in body axes velocities, calculated above, must be added to the IMU sensed velocities.

$$V_x = V_x' + \Delta V_x$$

$$V_y = V_y' + \Delta V_y$$

$$V_z = V_z' + \Delta V_z$$

Accelerations about the IMU could be corrected in a similar way, but as explained previously, this isn't required. These same equations obviously can be used to determine the velocities and accelerations about any known point on the aircraft.

FLYING QUALITY AND PERFORMANCE CURVES

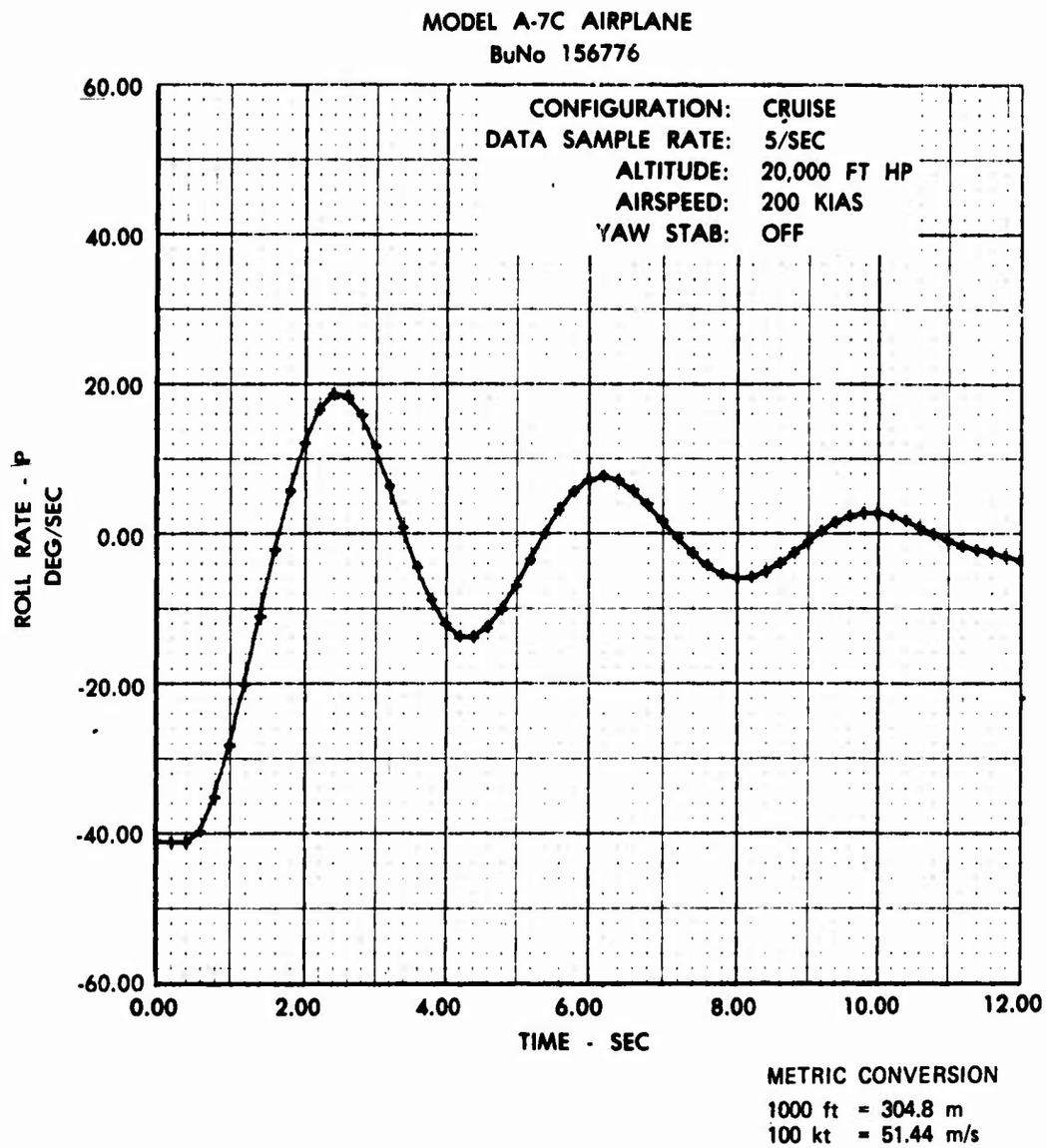

Figure 1
Dutch Roll Excitation

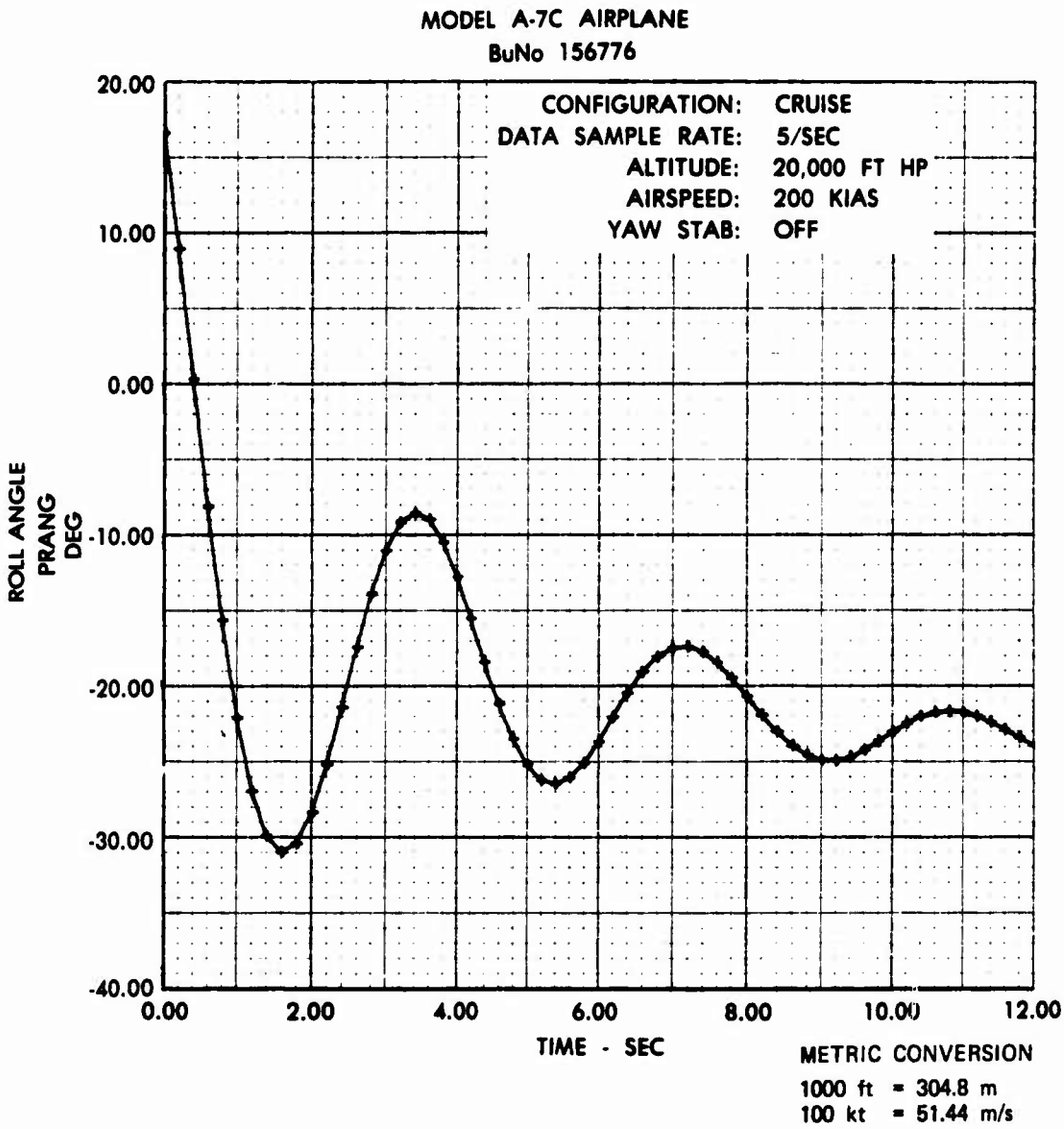

Figure 2
Dutch Roll Excitation

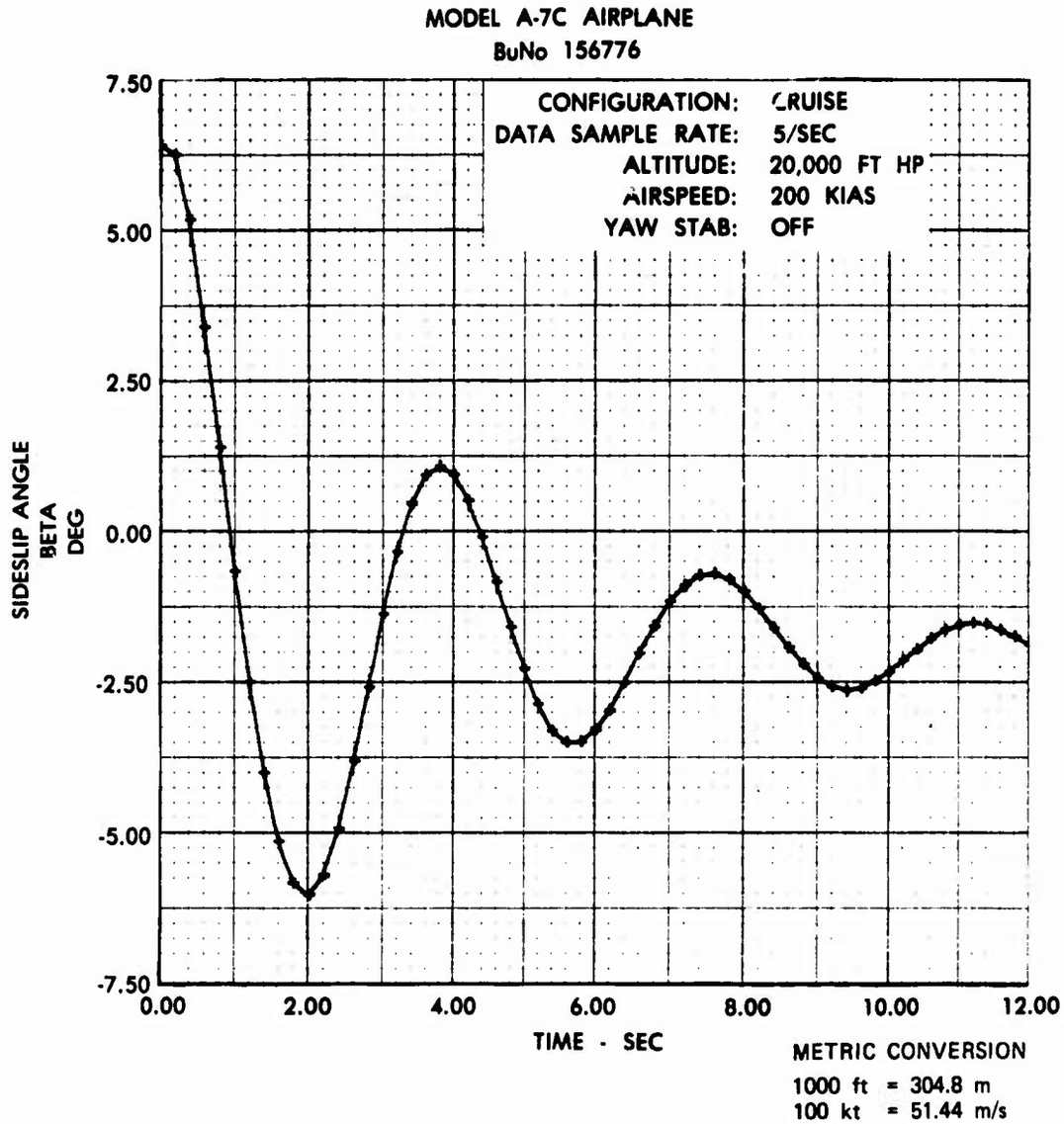

Figure 3
Dutch Roll Characteristics

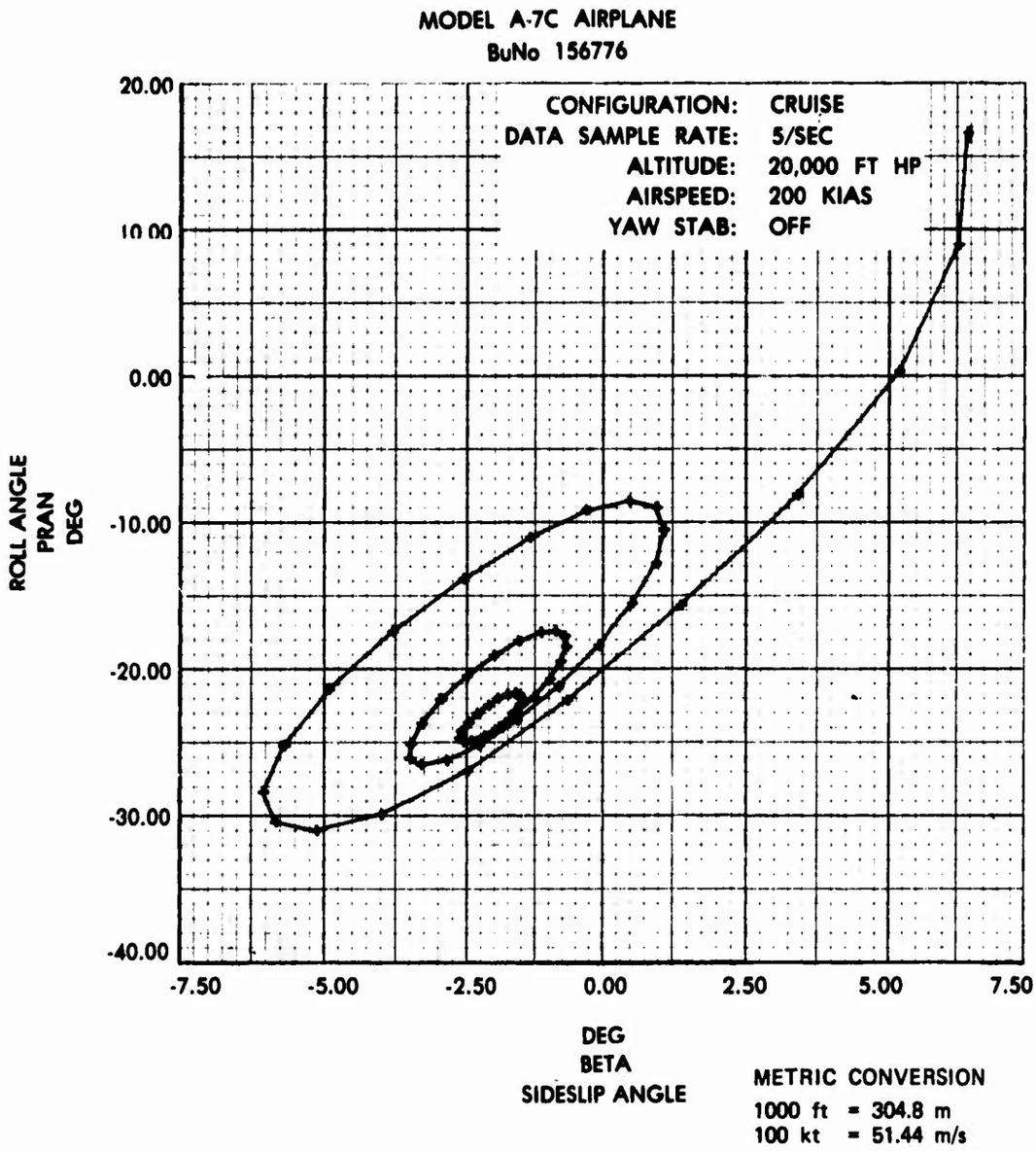

Figure 4
Dutch Roll Excitation

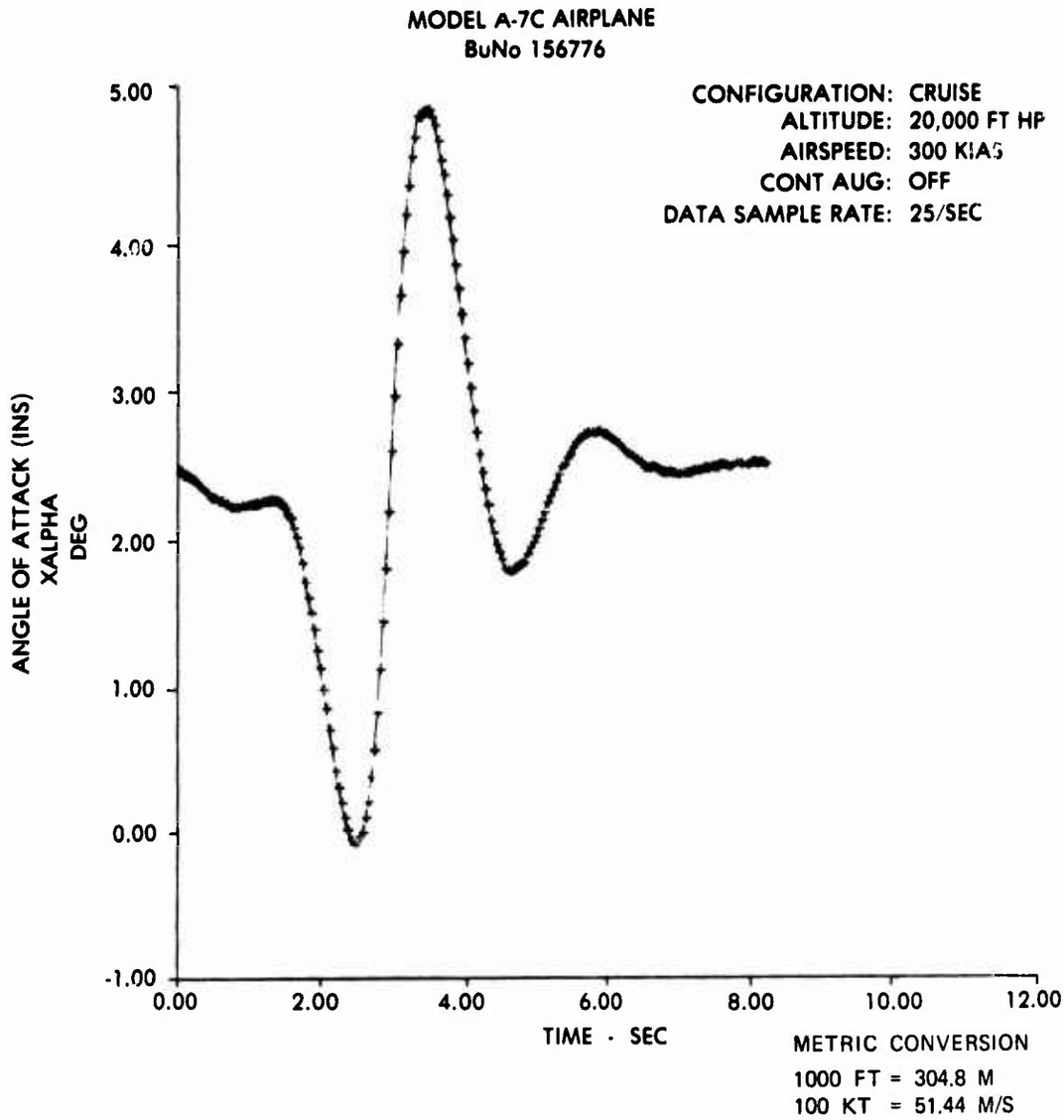

Figure 5
Short Period Excitation

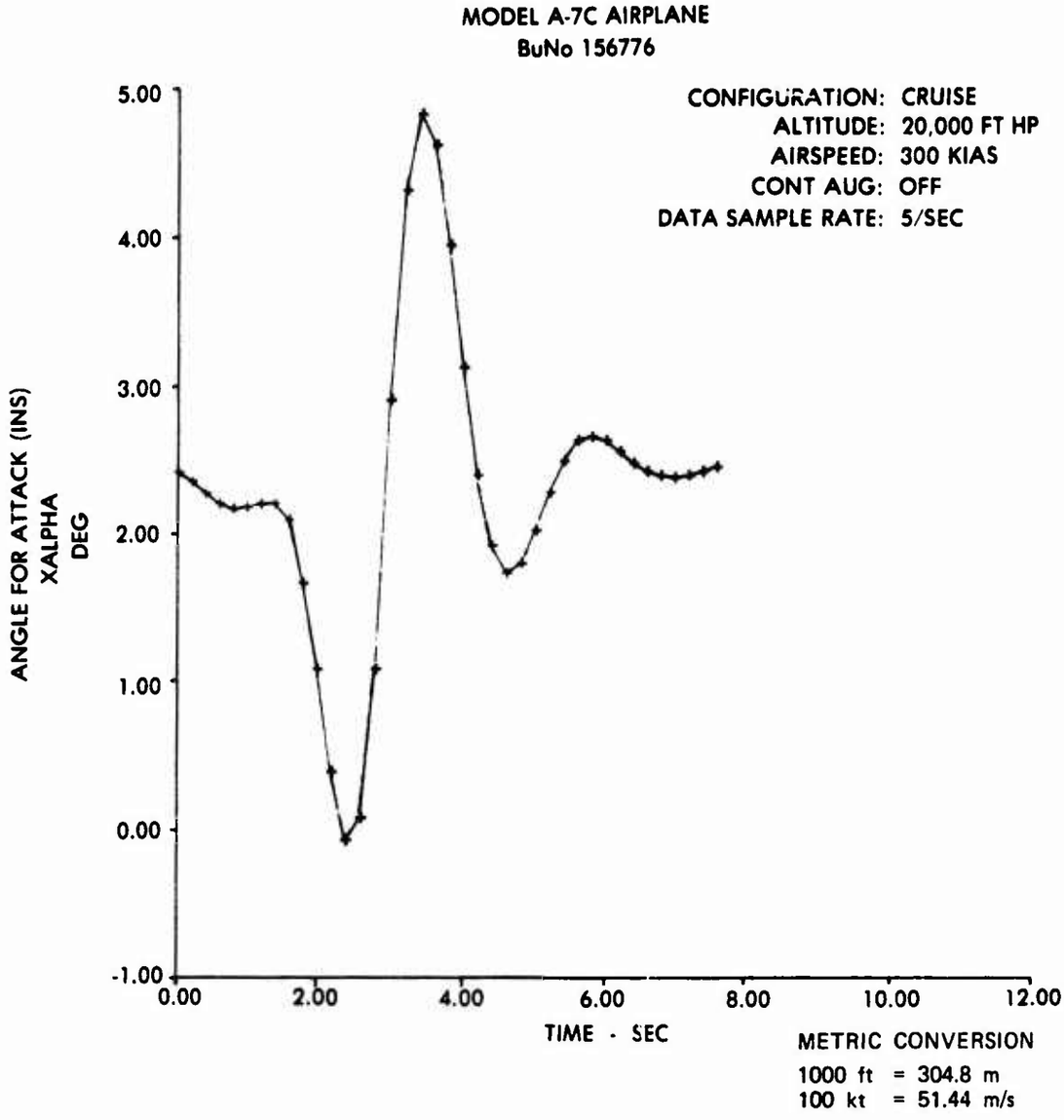

Figure 6
Short Period Excitation

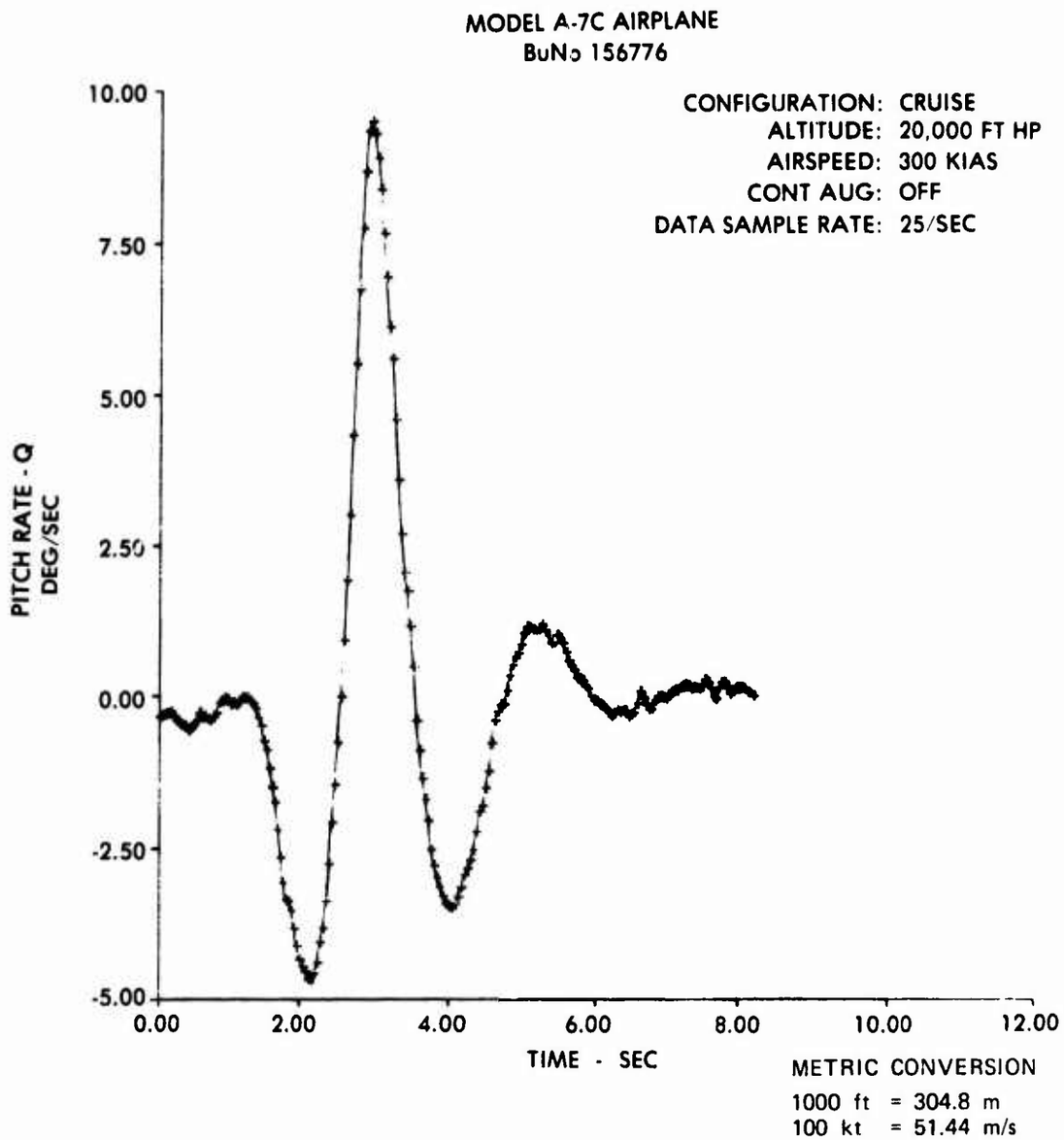

Figure 7
Short Period Excitation

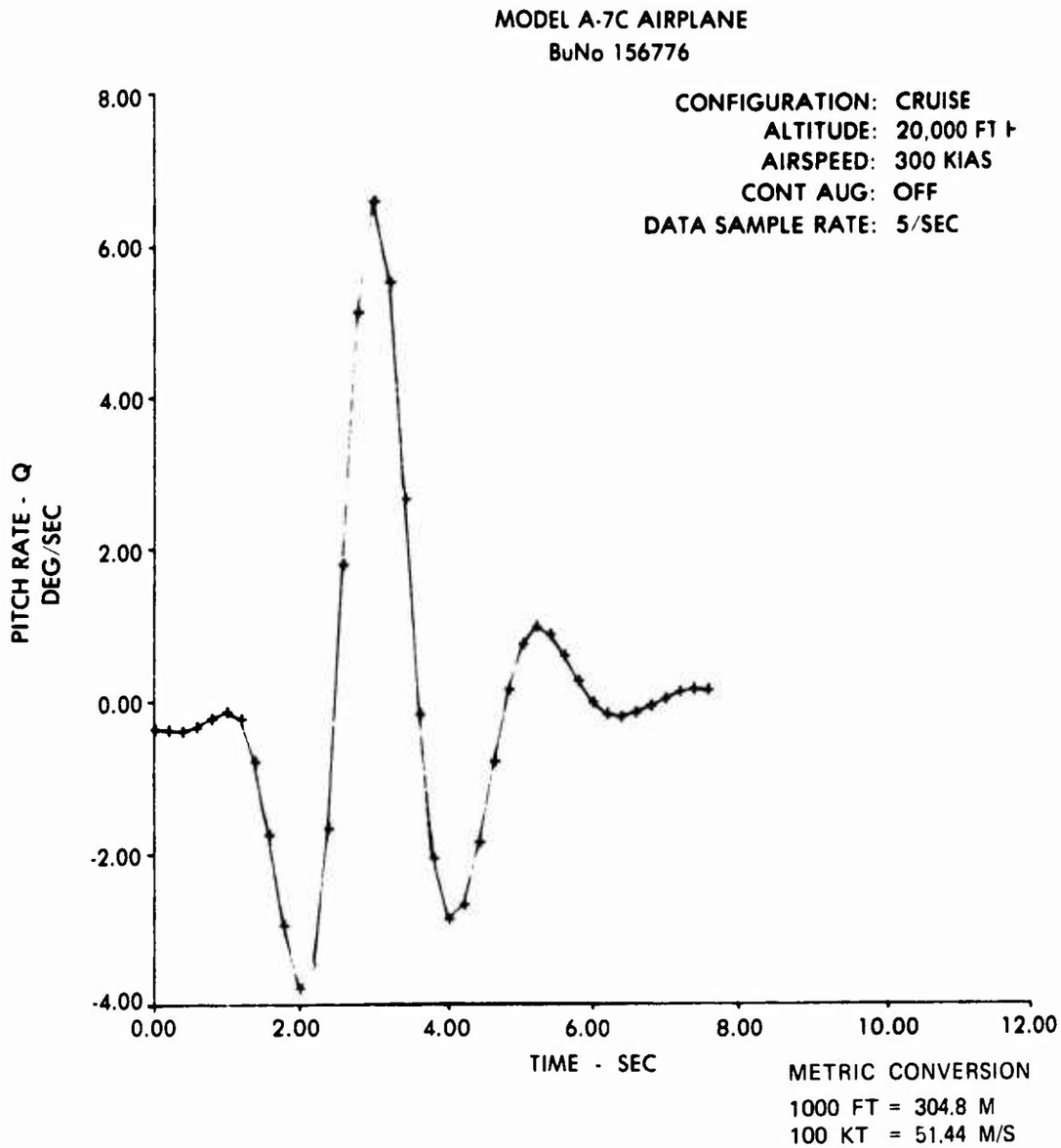

Figure 8
Short Period Excitation

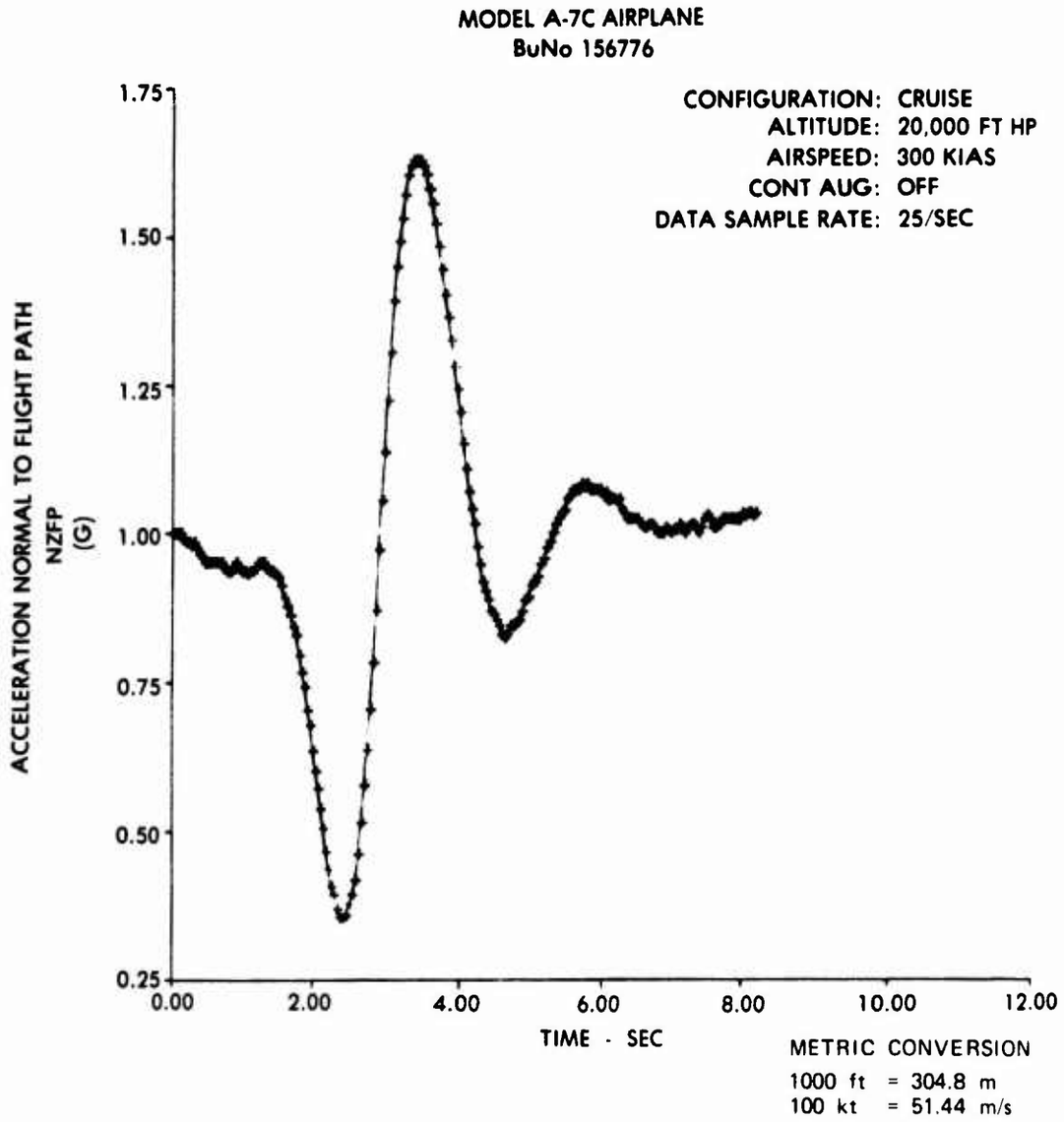

Figure 9
Short Period Excitation

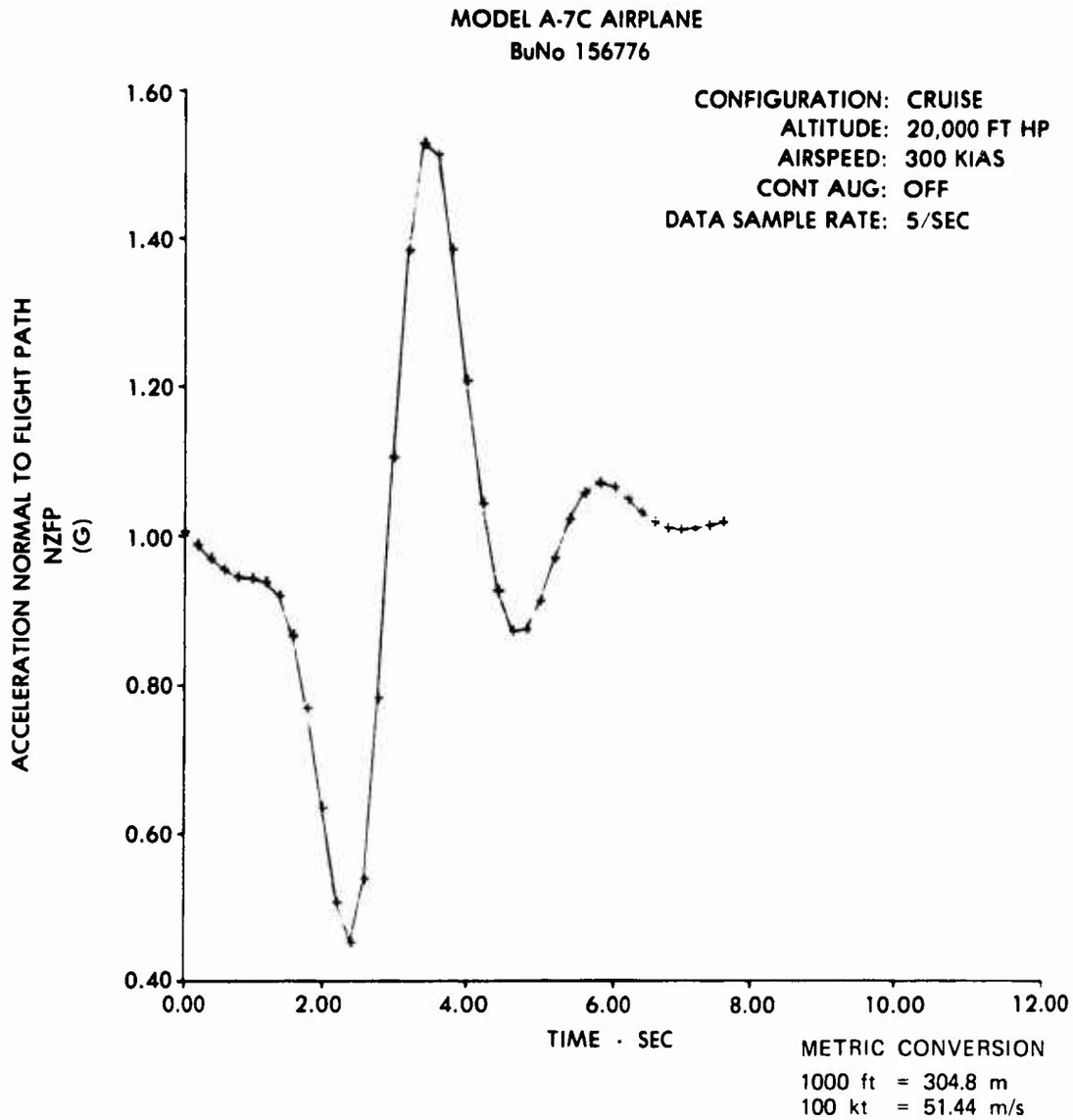

Figure 10
Short Period Excitation

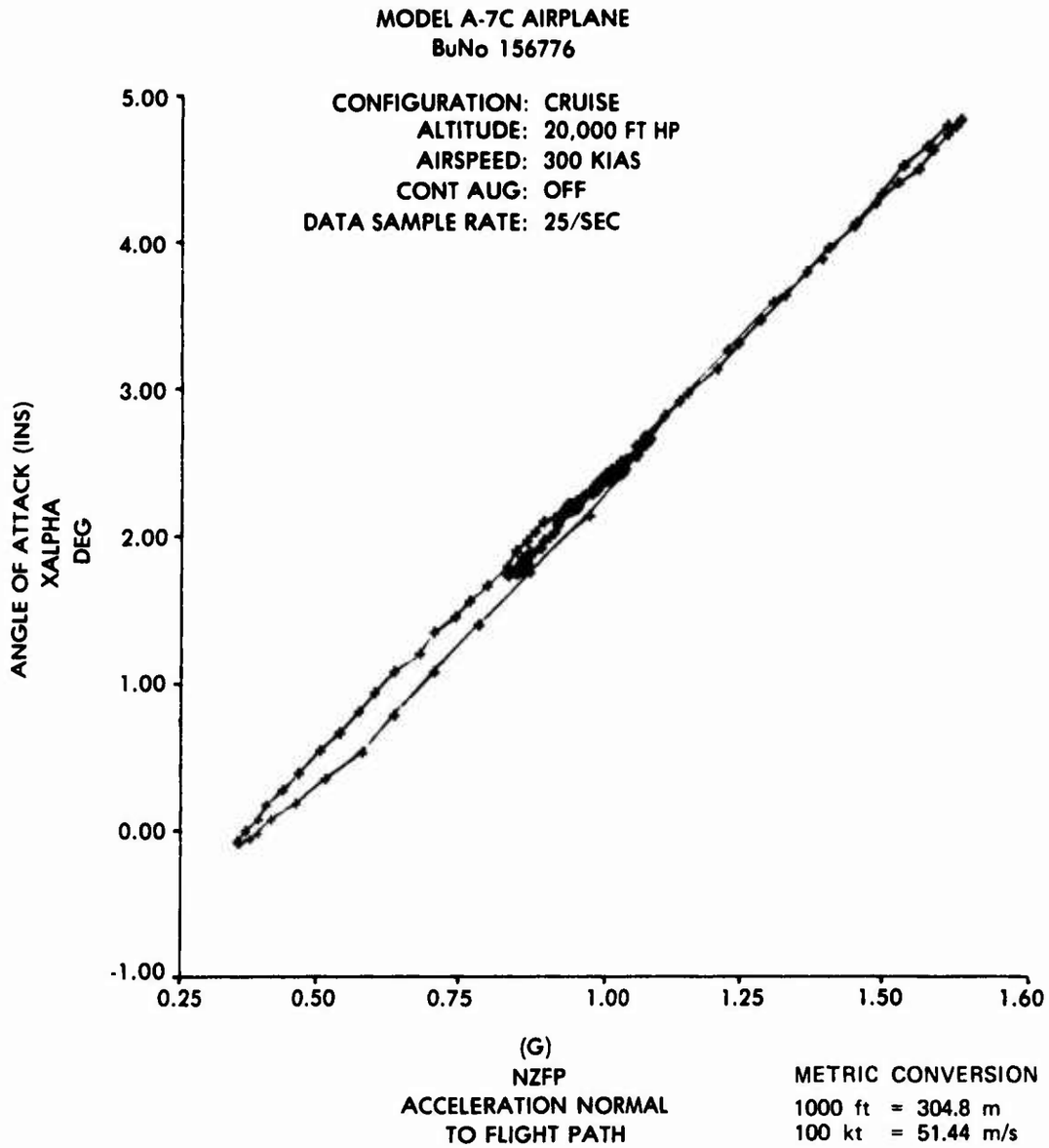

Figure 11
Short Period Excitation

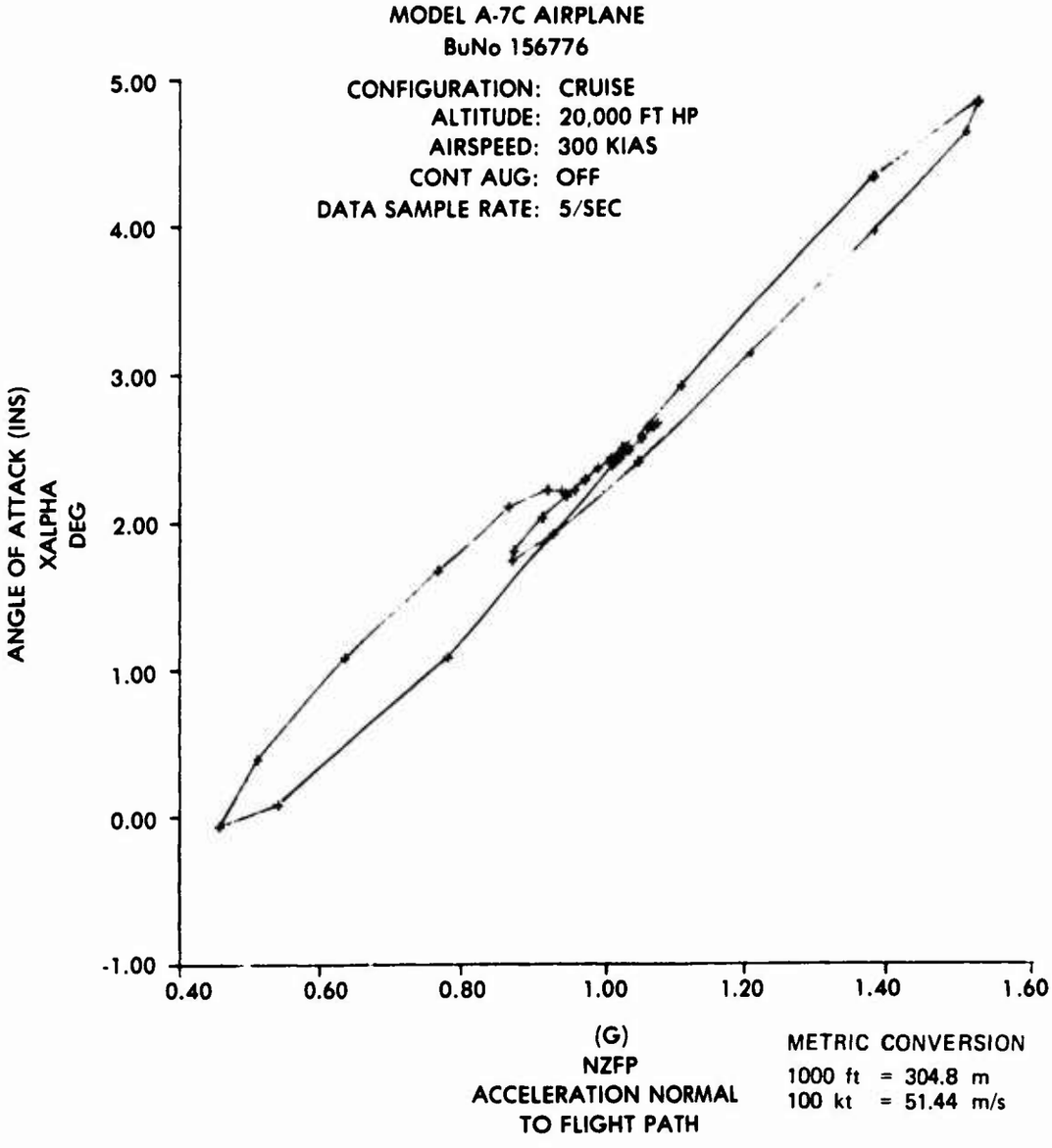

Figure 12
Short Period Excitation

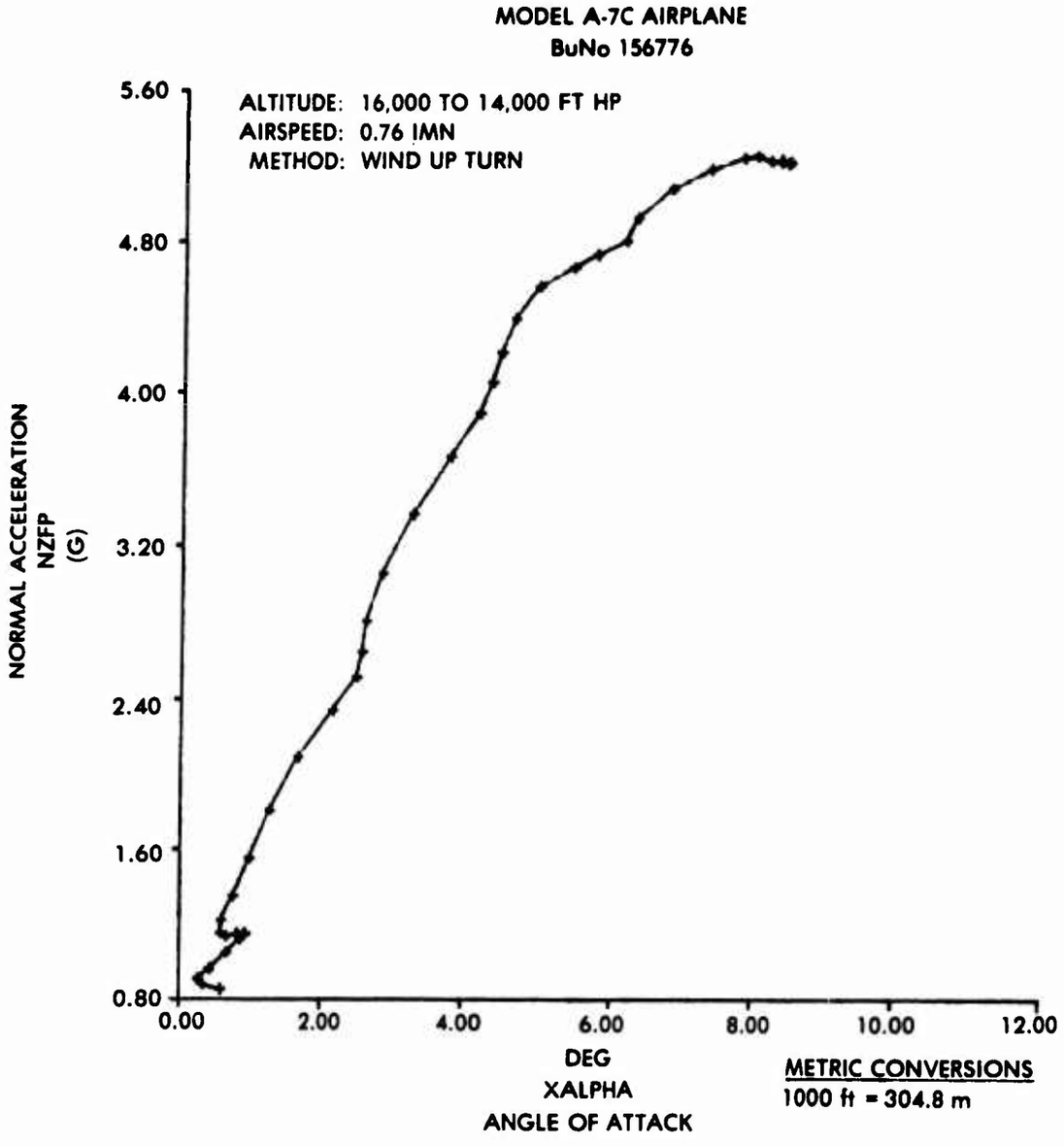

Figure 13
Maneuvering Stability

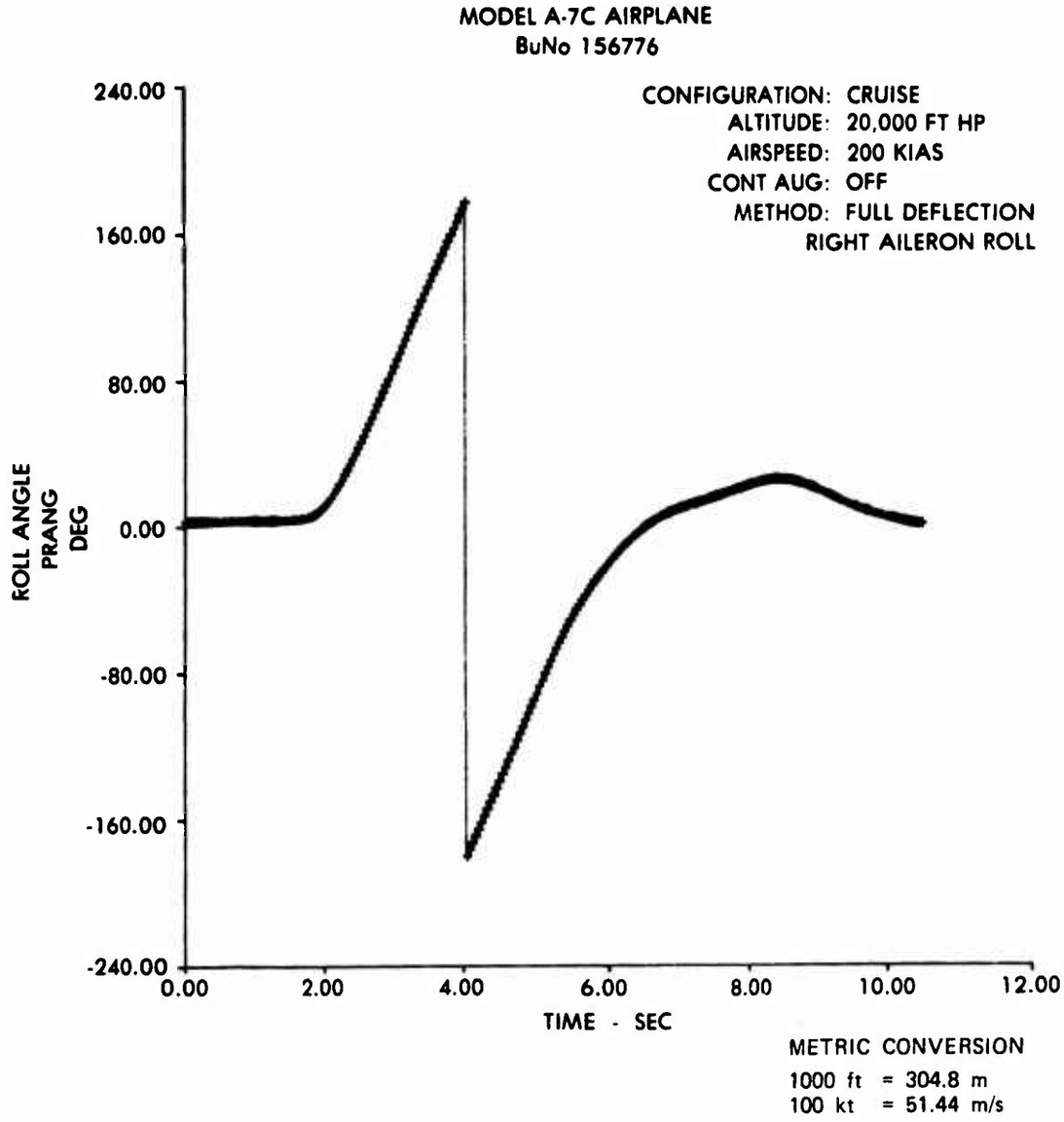

Figure 14
Roll Performance

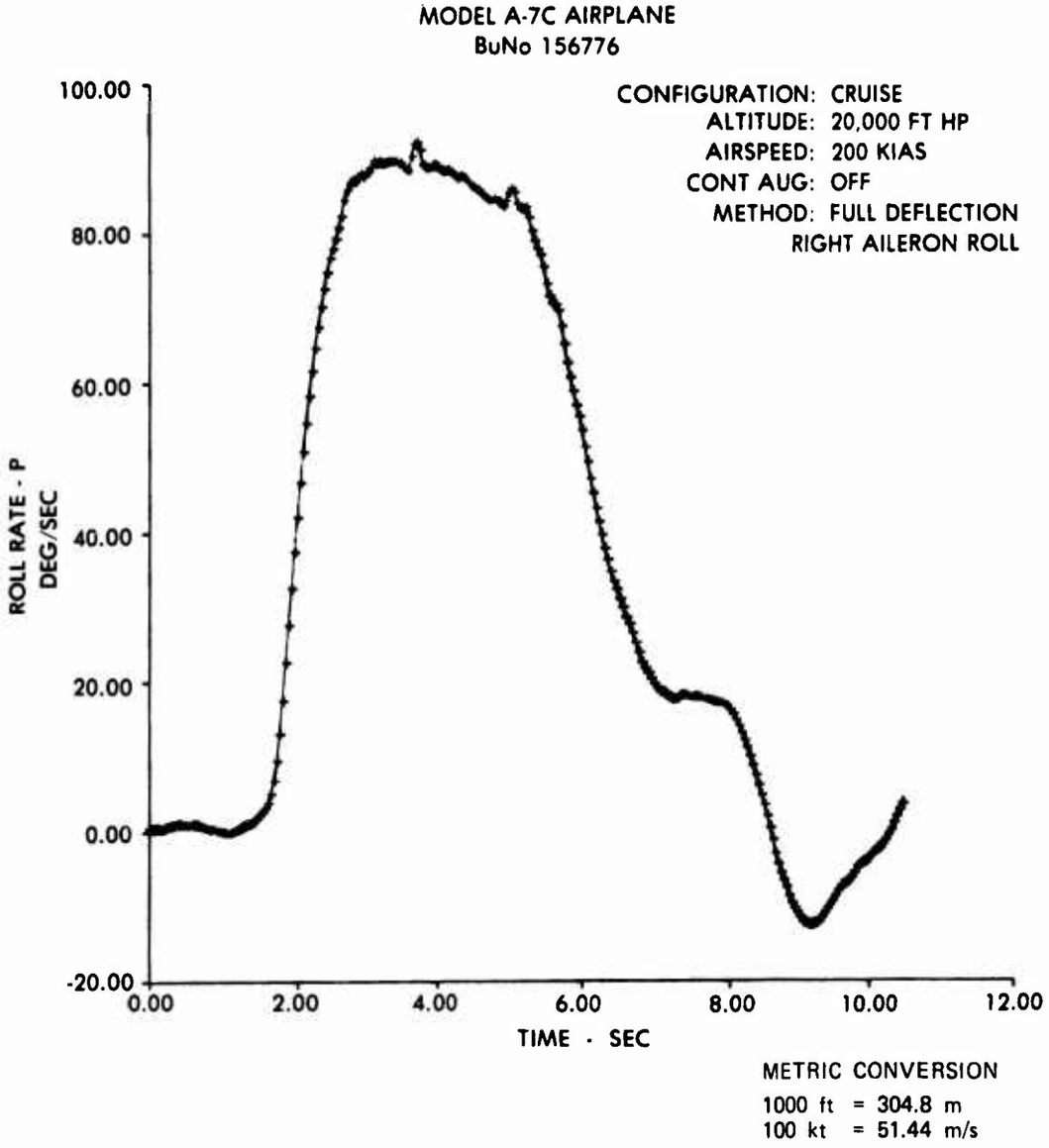

Figure 15
Roll Performance

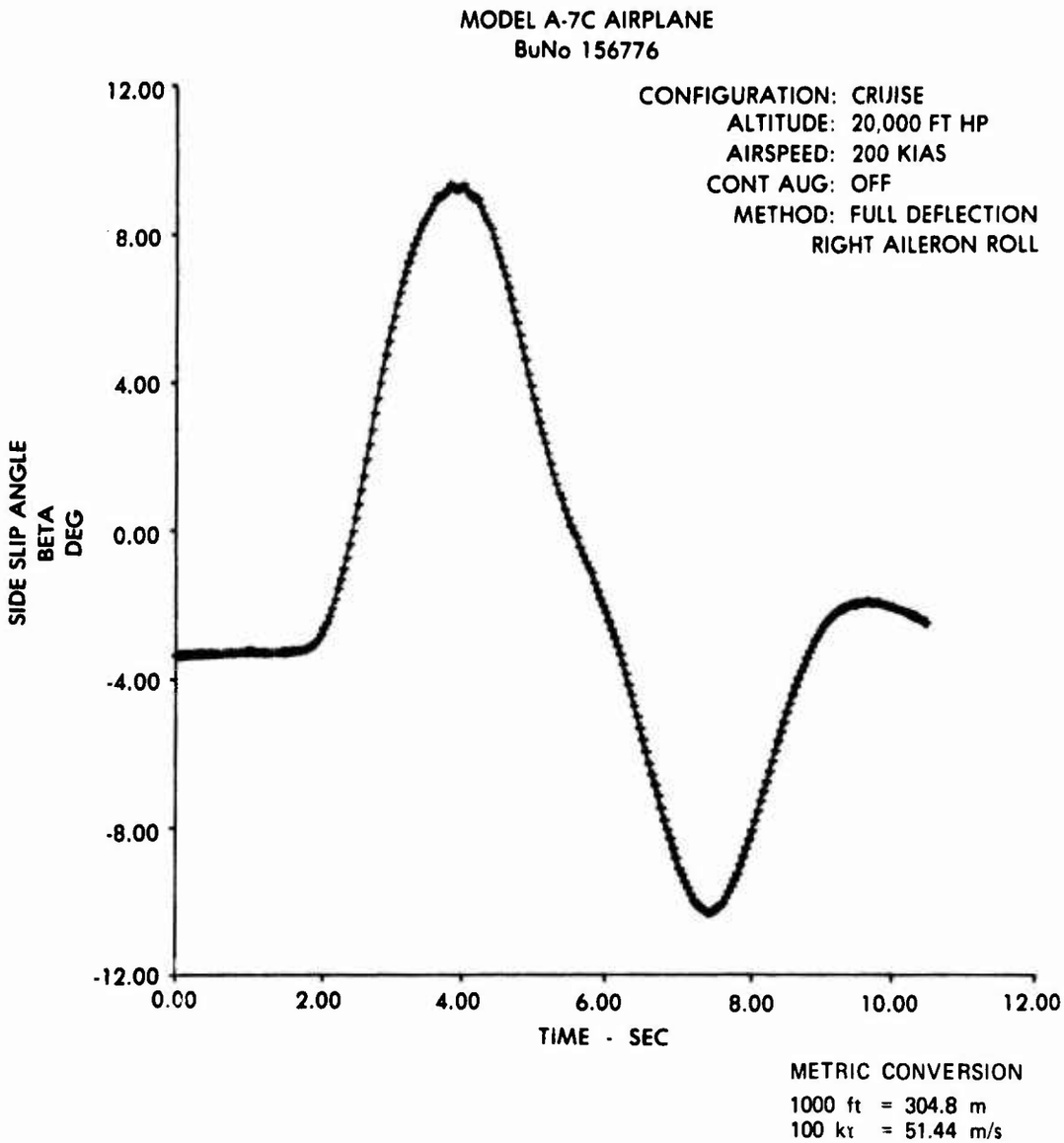

Figure 16
Roll Performance

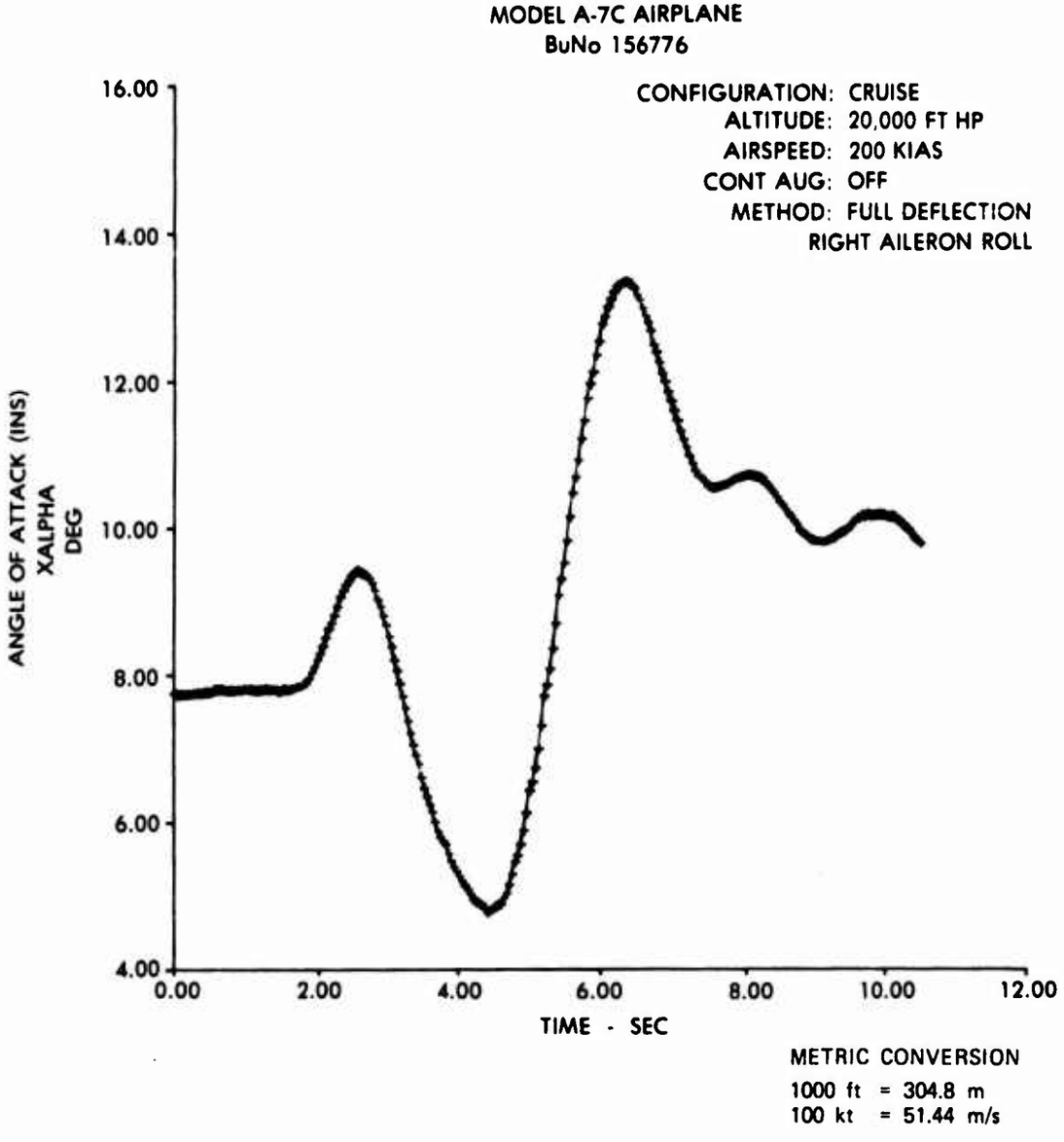

Figure 17
Roll Performance

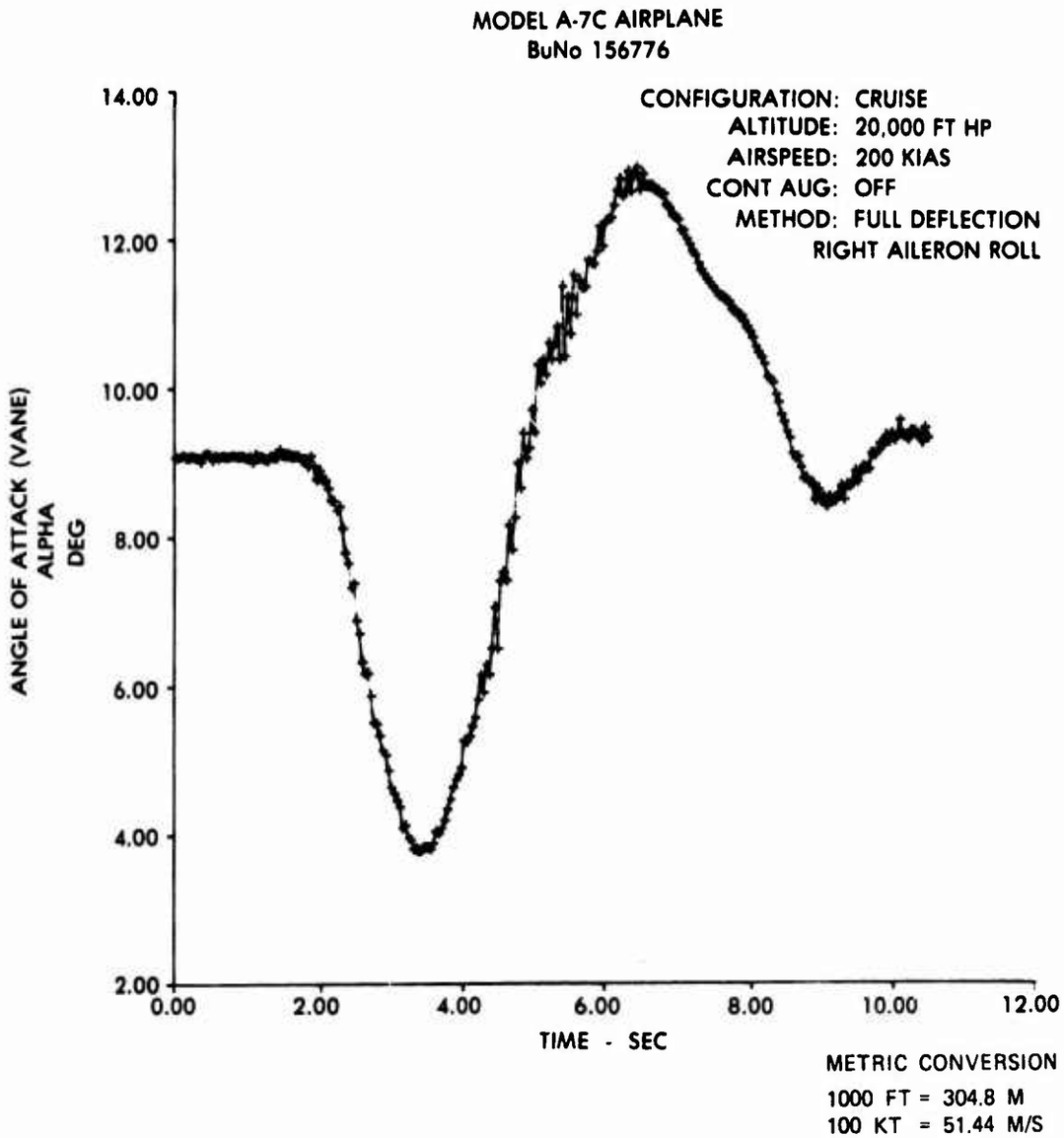

Figure 18
Roll Performance

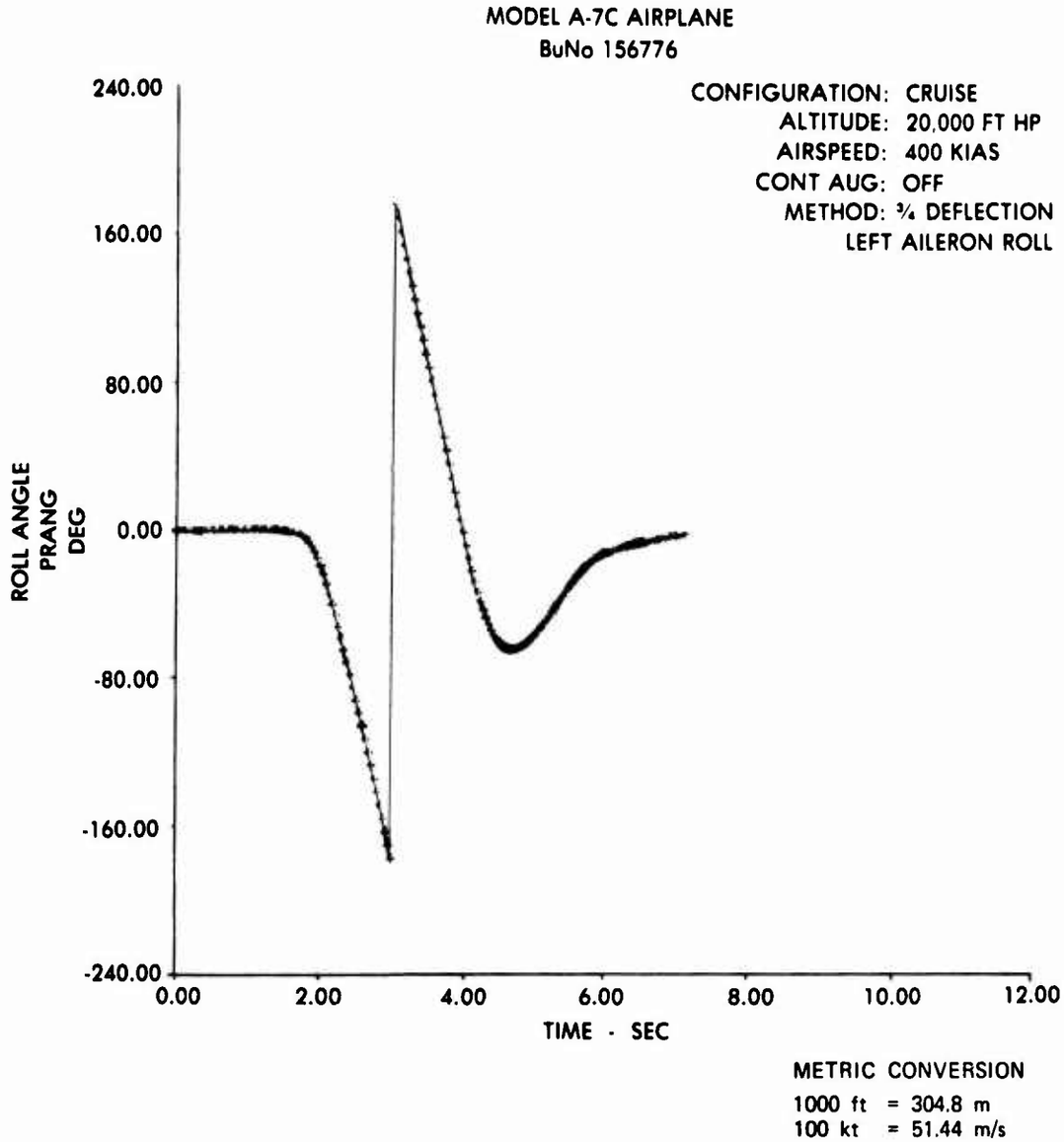

Figure 19
Roll Performance

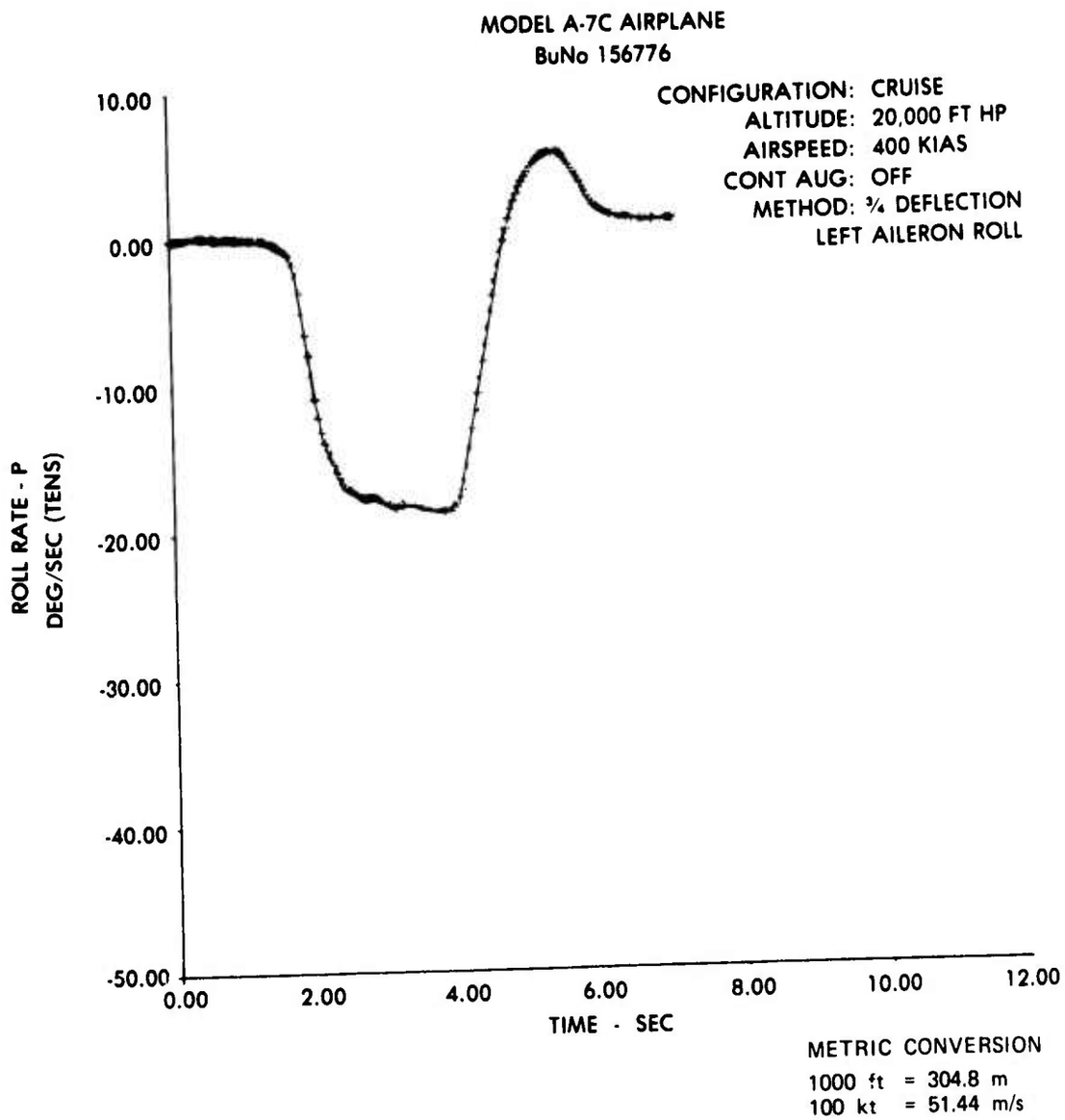

Figure 20
Roll Performance

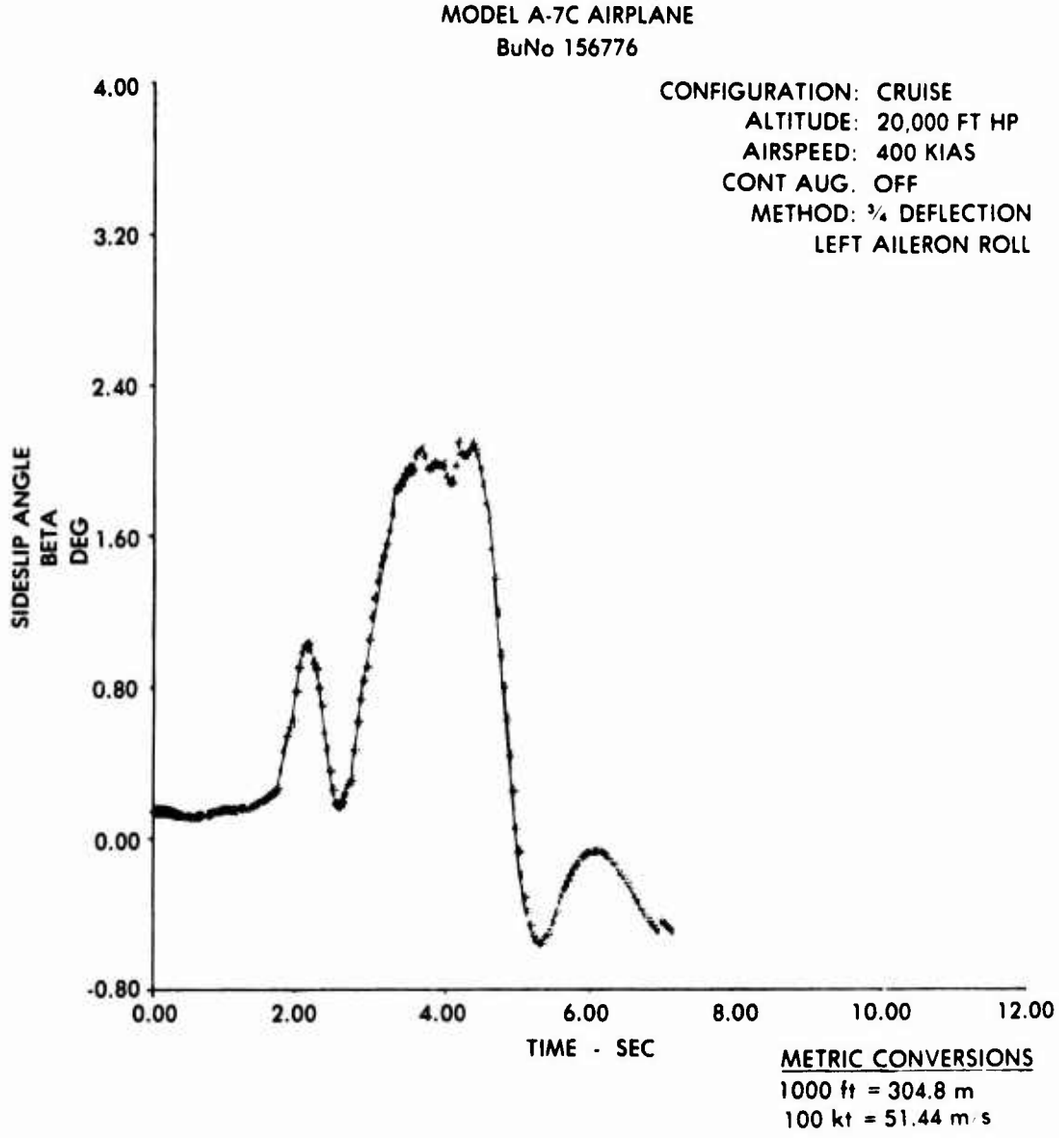

Figure 21
Roll Performance

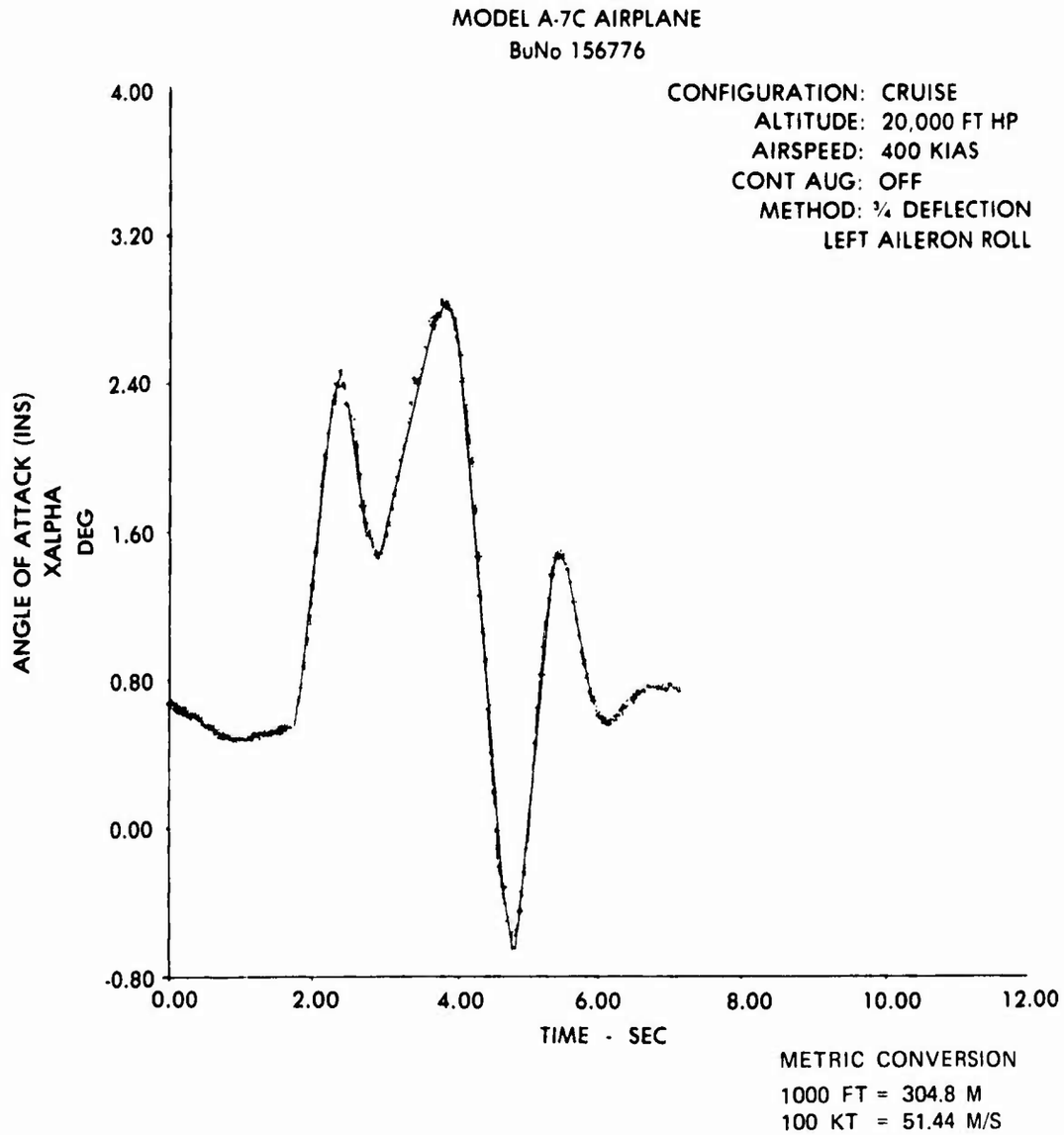

Figure 22
Roll Performance

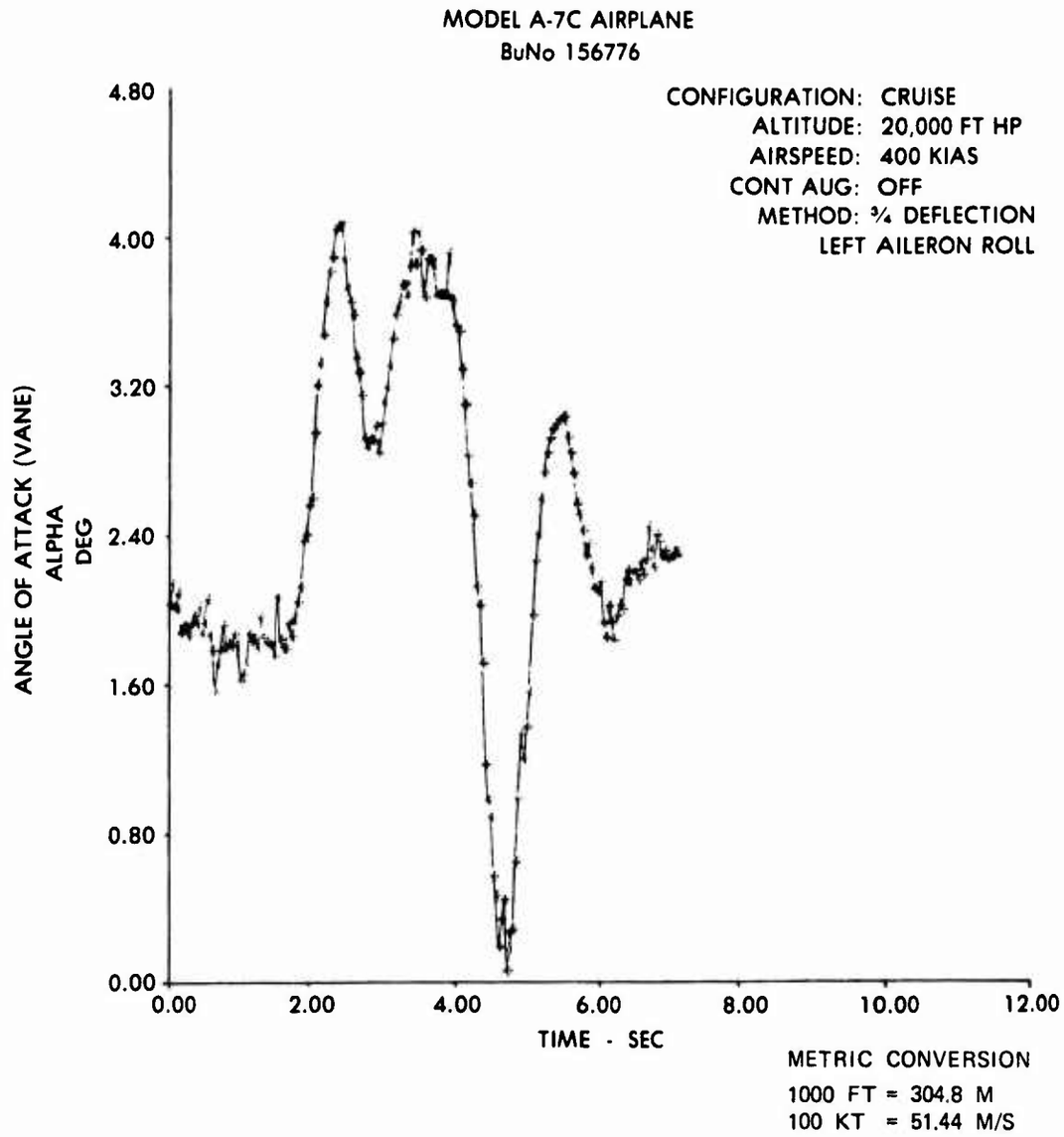

Figure 23
Roll Performance

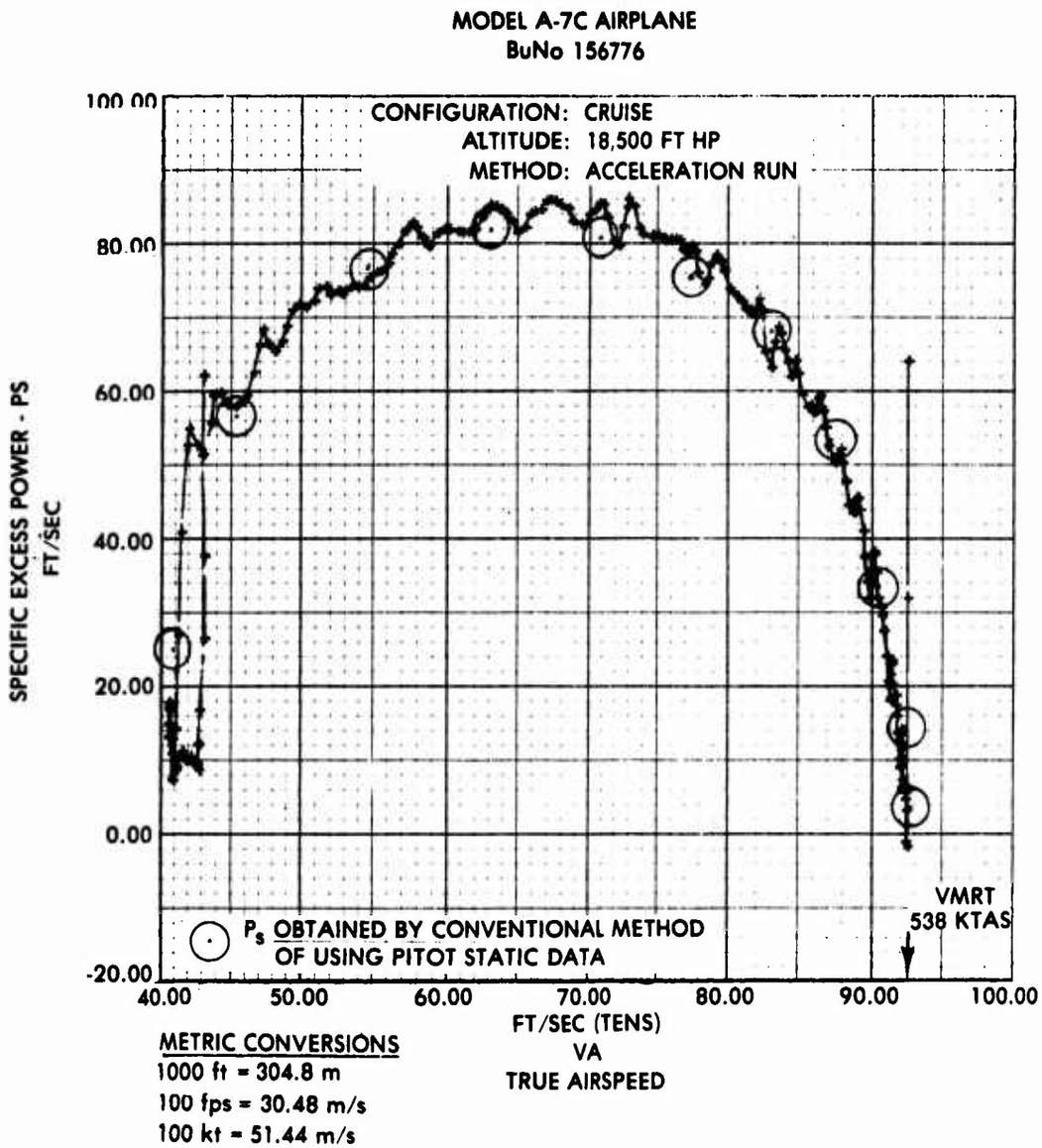

Figure 24
Specific Excess Power

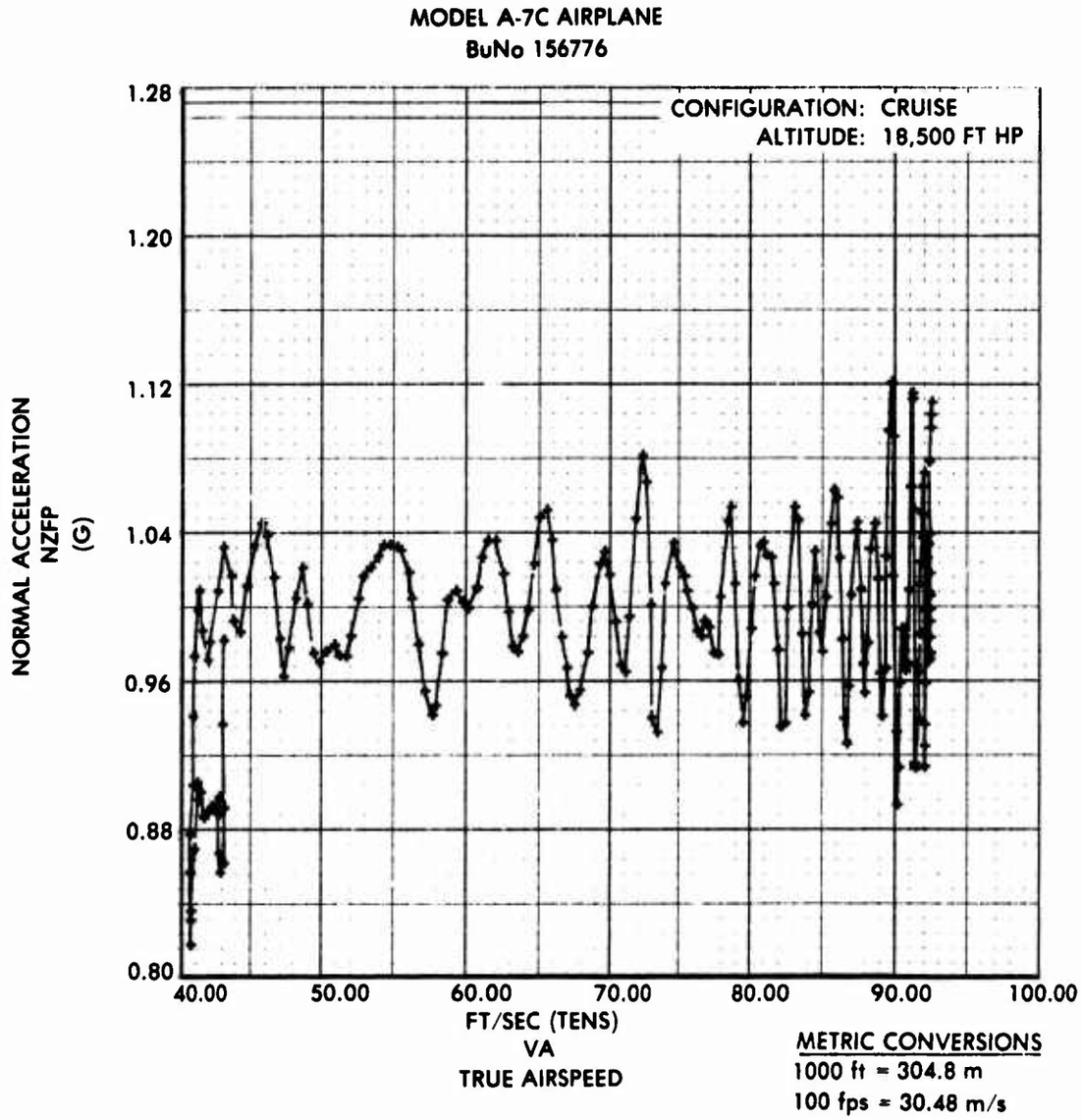

Figure 25
Acceleration Run

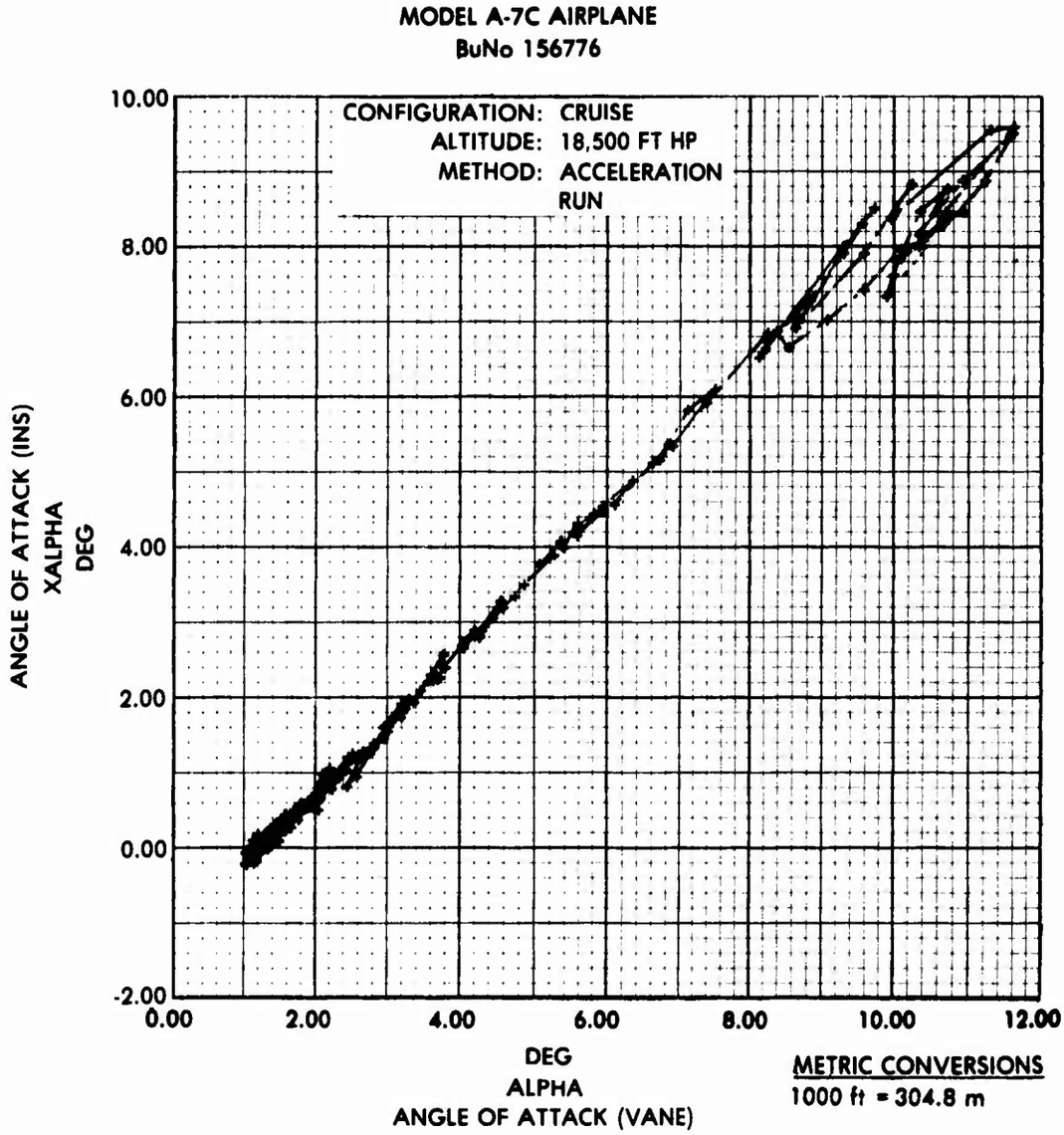

Figure 26
Angle of Attack Correlation

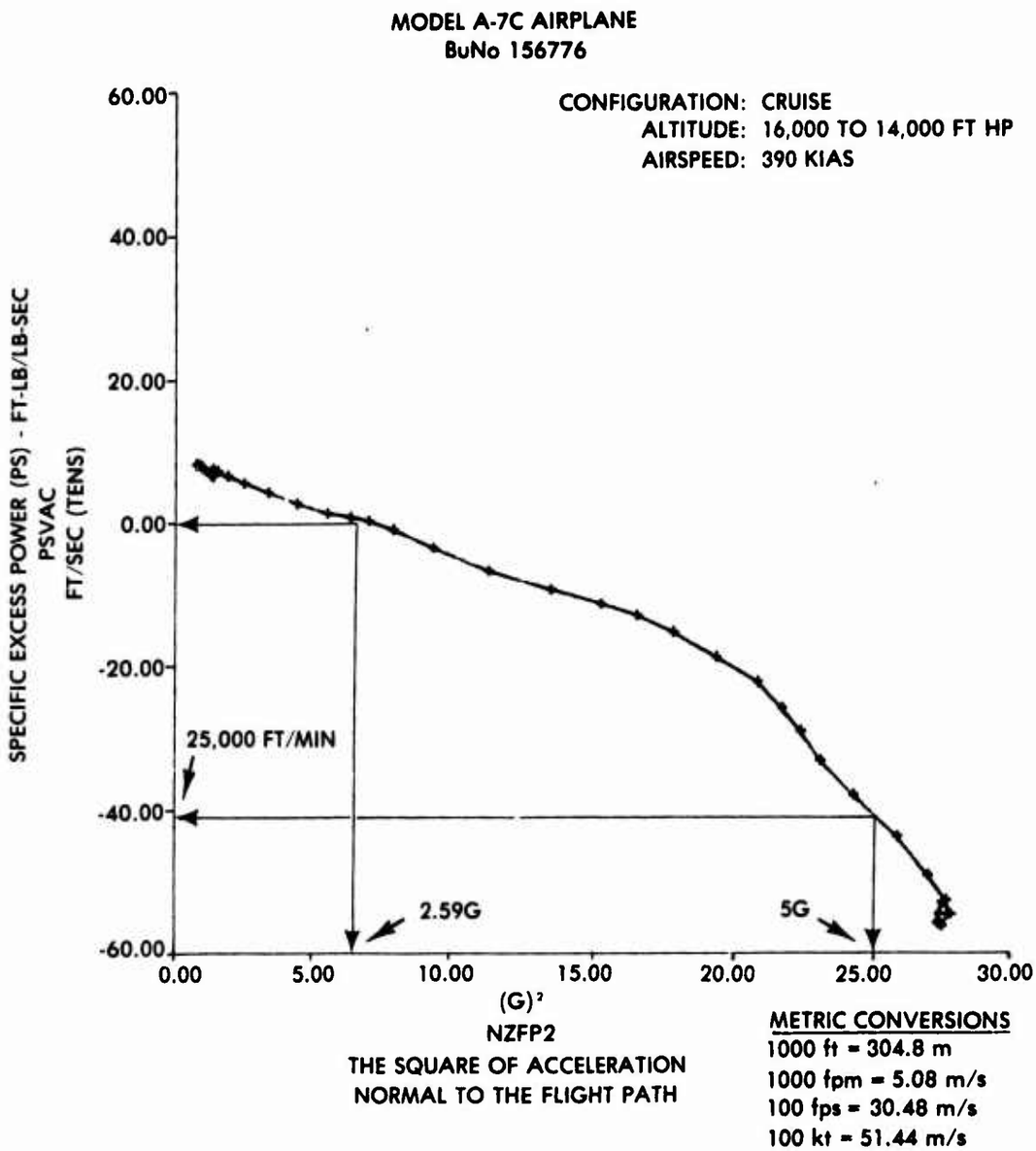

Figure 27
Maneuvering Performance

LIST OF ABBREVIATIONS AND SYMBOLS

ADC - Air Data Computer

AFP - Acceleration Along the Flight Path

AFPI - Acceleration Along the Flight Path - Indicated

AYI - Indicated Lateral Acceleration

A - Acceleration

A_N - Acceleration Along the North Axis

A_E - Acceleration Along the East Axis

A_V - Acceleration Along the Vertical Axis (positive down)

A_x - Acceleration Along the Airplane's x Axis

A_y - Acceleration Along the Airplane's y Axis

A_z - Acceleration Along the Airplane's z Axis

CEP - Circular Error Probable

D - Airplane Drag

FQ&P - Flying Qualities and Performance

g - Gravitational Constant (32.2 ft/sec^2 or 9.81 m/sec^2)

hr - Hour

H_p - Pressure Altitude

IFP - Inertially Derived Flying Qualities and Performance Parameters

IMU - Inertial Measurement Unit

INS - Inertial Navigation System

kg - Kilograms

km - Kilometer

kt - Knot

KTAS - True Airspeed - Knots

M - Mach Number

m - Meters

N - Acceleration Measured in "g" Units

NATC - Naval Air Test Center

nmi - Nautical Miles

NPV - North Pointing - Local Vertical Axis System

NZFP - Acceleration Normal to the Flight Path (in "g" Units)

P - Position

P_s - Specific Excess Power

p - Roll Rate Measured About the Airplane's x Axis

Q - Dynamic Pressure

q - Pitch Rate Measured About the Airplane's y Axis

R - Earth's Radius

r - Yaw Rate Measured About the Airplane's z Axis

S - Laplace Operator

s - Seconds

T - Thrust

USNTPS - U. S. Naval Test Pilot School

V - Velocity

V_{NI} - Inertial Velocity - North

V_{EI} - Inertial Velocity - East

V_{VI} - Inertial Velocity - Vertical

V_I - Airplane's Inertial Velocity Vector

V_N - Air Mass Referenced Velocity - North

V_E - Air Mass Referenced Velocity - East

V_V - Air Mass Referenced Velocity - Vertical

V_A - Magnitude of Air Mass Referenced Velocity (True Airspeed)

$\bar{V}_A$ - Airplane's Air Mass Referenced Velocity Vector

V_{AC} - Magnitude of Air Mass Referenced Velocity - Computed from "frozen" winds and inertial velocities

V_{WN} - Wind Velcoity - North

V_{WE} - Wind Velocity - East

V_{WV} - Wind Velocity - Vertical

V_W - Wind Velocity Vector

V_x - Component of Air Mass Referenced Velocity Along Airplane's x Axis

V_y - Component of Air Mass Referenced Velocity Along Airplane's y Axis

V_z - Component of Air Mass Referenced Velocity Along Airplane's z Axis

W - Airplane Gross Weight

x - Airplane's x Axis

y - Airplane's y axis

z - Airplane's z Axis

α - Angle of Attack

α_I - Inertially Derived Angle of Attack

α_B - Boom Measured Angle of Attack

α_E - Angle of Attack Error

β - Sideslip Angle

β_I - Inertially Derived Sideslip

β_B - Boom Measured Sideslip

β_E - Sideslip Error

γ - Flight Path Angle (Air Mass Referenced)

γ_I - Flight Path Angle (Earth Referenced)

ρ - Air Density

Special Symbols

$(\dot{})$ - Indicates First Derivative of Term in Parenthesis

$(\ddot{})$ - Indicates Second Derivative of Term in Parentheses

Δ - Change or Error in

$\vec{(\ )}$ - Indicates Vector

$\tilde{(\ )}$ - Indicates a Measured Quantity

$(\ )_o$ - Indicates Value of Quantity at "Wind Freeze" or Time Zero

X - Cross Product